EPITHELIAL-TO-MESENCHYMAL TRANSITION AND FIBROBLAST DIFFERENTIATION IN IDIOPATHIC PULMONARY FIBROSIS

By

XIAO XIAO

Bachelor of Medicine in Clinical Medicine
Sun Yat-Sen University
Guangzhou, Guangdong, China
2007

Master of Medicine in Ophthalmology
Sun Yat-Sen University
Guangzhou, Guangdong, China
2009

Submitted to the Faculty of the
Graduate College of the
Oklahoma State University
in partial fulfillment of
the requirements for
the Degree of
DOCTOR OF PHILOSOPHY
December, 2015

EPITHELIAL-TO-MESENCHYMAL TRANSITION

AND FIBROBLAST DIFFERENTIATION IN

IDIOPATHIC PULMONARY FIBROSIS

Dissertation Approved:

Dr. Lin Liu

Dissertation Adviser

Dr. Myron Hinsdale

Dr. Chris Ross

Dr. Junpeng Deng

Name: XIAO XIAO

Date of Degree: DECEMBER, 2015

Title of Study: EPITHELIAL-TO-MESENCHYMAL TRANSITION AND FIBROBLAST DIFFERENTIATION IN IDIOPATHIC PULMONARY FIBROSIS

Major Field: Veterinary Biomedical Sciences (Physiology)

Abstract:

The aim of the present study is to explore the molecular mechanisms of epithelial-to-mesenchymal transition and fibroblast differentiation during the pathogenesis of idiopathic pulmonary fibrosis.

We identified 6 up-regulated and 3 down-regulated miRNAs in a human lung epithelial cell EMT model using miRNA microarray and real-time PCR. Overexpression of one of these up-regulated miRNAs, miR-424, increased the expression of α-smooth muscle actin, an indicator of myofibroblast differentiation, but had no effects on the epithelial or mesenchymal cell markers. miR-424 enhanced the activity of the TGF-β signaling pathway, as demonstrated by a luciferase reporter assay. Further experiments showed that miR-424 decreased the protein expression of Smurf2, a negative regulator of TGF-β signaling, indicating that miR-424 exerts a forward regulatory loop in the TGF-β signaling pathway. Our results suggest that miR-424 regulates the myofibroblast differentiation during EMT by potentiating the TGF-β signaling pathway, likely through Smurf2.

Furthermore, we investigated the role of EZH2 in the differentiation of fibroblasts into myofibroblasts and underlying mechanisms. We found that EZH2 was up-regulated in the lungs of patients with IPF and mice with bleomycin-induced lung fibrosis. The up-regulation of EZH2 occurred in myofibroblasts. The inhibition of EZH2 by its inhibitor DZNep or shRNA reduced TGFβ1-induced differentiation of human lung fibroblasts into myofibroblasts as demonstrated by the expression of myofibroblast marker α-smooth muscle actin, fibronectin and COL4A1 as well as contractility. DZNep inhibited Smad2/3 nuclear translocation without affecting Smad2/3 phosphorylation. Co-immunoprecipitation revealed a direct interaction between EZH2 and Smad2/3. DZNep treatment attenuated bleomycin-induced pulmonary fibrosis in mice. We conclude that EZH2 induces the differentiation of fibroblasts to myofibroblasts by binding and retaining Smad2/3 in the nucleus.

TABLE OF CONTENTS

Chapter Page

LIST OF TABLES

Table Page

LIST OF FIGURES

Figure Page

LIST OF ABBREVIATIONS

3'-UTR	Three prime untranslated region
ABC	Avidin-biotin complex
AdoHcy	S-adenosylhomocysteine
AEC	Alveolar epithelial cells
ANOVA	Analysis of variance
BCP	1-bromo-3-chloropropane
bHLH	Basic helix-loop-helix
BMI	Body-mass index
C/EBPβ	CCAAT/enhancer binding protein β
CDH1	Cadherin 1, Type 1
CDH2	Cadherin 2, Type 1
CDKs	Cyclin-dependent kinases
cDNA	Complementary DNA
Co-IP	Co-Immunoprecipitation
COL1A1	Collagen, Type I, Alpha 1
COL3A1	Collagen, Type III, Alpha 1
COL4A1	Collagen, Type IV, Alpha 1
COX-2	Cyclooxygenase 2
CT	Threshold cycle
CTGF	Connective tissue growth factor
CXCL12	Chemokine (C-X-C Motif) Ligand 12
CXCR4	Chemokine (C-X-C Motif) Receptor 4
DKC1	Dyskeratosis Congenita 1, Dyskerin
DMEM	Dulbecco's Modified Eagle's Medium
DNA	Deoxyribonucleic acid
DZNep	3-Deazaneplanocin A
ECL	Enhanced chemiluminescence
ECM	Extracellular matrix
EDTA	Ethylenediaminetetraacetic acid
EED	Embryonic ectoderm development
EMT	Epithelial-to-mesenchymal transition
ER	Endoplasmic reticulum
EZH2	Enhancer of zeste homolog 2

F-12K medium	Kaighn's Modification of Ham's F-12 Medium
FBS	Fetal bovine serum
FDA	Food and Drug Administration
FGF	Fibroblast growth factor
FN	Fibronectin
FVC	Forced vital capacity
FW	Forward
GER	Gastroesophageal reflux
GFP	Green fluorescent protein
H3K27me3	Trimethylation of histone H3 lysine 27
HEK 293 ccells	Human Embryonic Kidney 293 cells
HMGA2	High Mobility Group AT-Hook 2
HRCT	High-resolution computed tomography
IFN-γ	Gamma interferon
ILD	Interstitial lung disease
Imp7	Importin 7
Imp8	Importin 8
IP-10	Gamma interferon (IFN-γ)-inducible protein of 10 kDa
IPF	Idiopathic pulmonary Fibrosis
Let-7d	Lethal-7d
LPA2	Lysophosphatidic acid receptor 2
LTRC	Lung Tissue Research Consortium
MAPK	Mitogen-activated protein kinases
miRNA	microRNA
MOI	Multiplicity of infection
mRNA	Messenger RNA
Msk	Moleskin
MUC5B	Mucin 5B, Oligomeric Mucus/Gel-Forming
NLS	Nuclear localization sequence
Nup153	Nucleoporin 153kDa
NUP214	Nucleoporin 214kDa
PBS	Phosphate-buffered saline
PCR	Polymerase chain reaction
PDGF	Platelet-derived growth factor
PRC2	Polycomb Repressive Complexes 2
p-Smads	Phosphorylated Smads
RBBP4	Retinoblastoma binding protein 4
RBBP7	Retinoblastoma binding protein 7
RE	Reverse
RISC	RNA-induced silencing complex
RNA	Ribonucleic acid

R-Smads	Receptor-activated Smads
SBEs	Smad3-binding elements
shRNA	Small hairpin RNA
SIP1	Smad interacting protein 1
Smad2	Mothers against decapentaplegic homolog 2
Smad3	Mothers against decapentaplegic homolog 3
Smad4	Mothers against decapentaplegic homolog 4
Smad7	Mothers against decapentaplegic homolog 7
Smurf1	SMAD specific E3 ubiquitin protein ligase 1
Smurf2	SMAD specific E3 ubiquitin protein ligase 2
SP-C	Surfactant Protein C
SUZ12	Suppressor of zeste 12
TAZ	PDZ-binding motif
TERC	Telomerase RNA component
TERT	Telomerase Reverse Transcriptase
TGF-β	Transforming growth factor beta
Thy-1	Thymocyte antigen 1
TRE	Transcription response element
TTBS	Tris-Buffered Saline with Tween 20
TβRI	TGFβ type I receptor
TβRII	TGFβ type II receptor
UIP	Usual interstitial pneumonia
UPR	Unfolded protein response
VEGF	Vascular endothelial growth factor
YAP	Yes-associated protein
YY1	YinYang1
ZEB1	Zinc finger E-box-binding homeobox 1
α-SMA	Alpha smooth muscle actin

CHAPTER I

INTRODUCTION

1.1 Idiopathic pulmonary fibrosis

Idiopathic pulmonary fibrosis (IPF) is a specific form of chronic, progressive fibrosing interstitial pneumonia and is associated with the histopathologic and radiologic pattern of usual interstitial pneumonia (UIP) [1, 2]. IPF is one of the most common forms of interstitial lung disease (ILD) which requires the exclusion of ILD associated with environmental exposure, medication, or systemic disease [1, 3]. IPF is characterized by deterioration of respiratory functions due to fibrosis of the lung interstitium. The clinical features include chronic exertional dyspnea, dry cough, bibasilar inspiratory crackles, and digital clubbing [1]. The criteria for the diagnosis of IPF include: 1) exclusion of other known causes of ILD; 2) the presence of a UIP pattern on high-resolution computed tomography (HRCT) in patients not subjected to surgical lung biopsy; and 3) Specific combinations of HRCT and surgical lung biopsy patterns in patients subjected to surgical lung biopsy [1]. The features of UIP on HRCT are subpleural, basal predominance, reticular abnormality, and honeycombing [1]. Histopathological criteria for UIP are composed of fibroblastic foci, patchy of fibrosis, and architectural distortion with honeycombing [1]. In the USA, the prevalence of IPF is estimated to be 14 - 27.9 cases per 100,000 population using narrow case definitions, and 42.7 - 63 per 100,000 population using broad case definitions. The annual incidence of IPF in the USA was estimated to be 6.8 - 8.8 per

100,000 population using narrow case definitions, and 16.3 - 17.4 per 100,000 population using broad case definitions [4].

The progression of disease has been described as a progressive decline in pulmonary function until eventual death from respiratory failure or complicating comorbidity [1]. The progression for each individual patient is unpredictable at the time of diagnosis. The majority of patients experience a slowly progressive decline over several to many years. Some of them remain stable or have an accelerated decline while others may have episodes of acute exacerbation [1]. The median survival time from diagnosis is 2 - 3 years according to several retrospective studies, and the mortality during 3-5 years after diagnosis is 50% [1, 5]. Worse prognosis has been associated with old age, smoking history, low body-mass index (BMI), digital clubbing, physiological impairment, UIP, and pulmonary hypertension [5, 6]. Most deaths (77%) in IPF are due to respiratory related causes including progression of IPF, acute exacerbation, acute lung injury, pneumonia and cor pulmonale. Other deaths (23%) are due to cardiac causes, sepsis, cancer, and other causes [5]. Potential risk factors are cigarette smoking [1, 7], ageing [8], environmental exposures to metal dusts (brass, lead, and steel) and wood dust (pine) [9, 10], chronic viral infection (Epstein-Barr virus and hepatitis C) [11-13], gastroesophageal reflux (GER) [14, 15], and diabetes mellitus [15].

Patients with IPF were traditionally treated with corticosteroid and immunosuppressant therapy and N-acetyl-cysteine until two studies showed negative results [16, 17]. Recently, two new medications, pirfenidone and nintedanib, have been approved by the U.S. Food and Drug Administration (FDA) for the treatment of IPF on October 2014. Pirfenidone inhibits fibroblast proliferation and collagen synthesis by regulating TGFβ and TNF-α whereas nintedanib inhibits the tyrosine kinase receptors for PDGF, VEGF and FGF. Both drugs have been shown to reduce the decline in forced vital capacity (FVC) [18].

The exact etiology of IPF is still unclear. Several studies have suggested that genetic predisposition is involved in IPF. Mutations in SFTPC gene and deficiency of SP-C were linked to IPF [19-23]. Mutations in SFTPC cause disruption of surfactant synthesis, which further induce protein misfolding and endoplasmic reticulum (ER) stress that produce the unfolded protein response (UPR) in alveolar epithelial type II cells. UPR induces apoptosis of alveolar type II cells, which disrupts the integrity of the alveolar epithelium [24-26]. Similarly, mutations of SFTPA2 have been associated with pulmonary fibrosis and lead to protein instability and ER stress [27, 28].

Telomerase mutations and telomere shortening are observed in patients with IPF. Mutations in the telomerase genes TERT and TERC have been found in both familial and sporadic cases [29-31]. Shorter telomeres have also been found in some IPF patients [32, 33]. Telomerase shortening may explain the increased occurrence of IPF in older individuals. Pulmonary fibrosis has been observed in a group of patients with dyskeratosis congenital, which have short telomeres due to DKC1 gene mutations [29, 30].

An increase in MUC5B gene common promoter polymorphism is associated with IPF [34, 35]. However, MUC5B is overexpressed even without the genetic variants, indicating another independent regulation of this gene may be involved.

Epigenetic regulation in IPF has also been studied. Abnormality in histone hypoacetylation in fibroblasts causes down-regulation of cyclooxygenase 2 (COX-2), which reduces the production of the antifibrotic protein prostaglandin E2 [36]. Histone deacetylation and hypermethylation are responsible for the repression of another antifibrotic gene gamma interferon (IFN-γ)-inducible protein of 10 kDa (IP-10) [37]. Other dysregulated genes due to abnormality in epigenetics include Thy-1, p14(ARF), and Fas [38-40]. Notably, methylation of 3 CpG islands in the promoter of the α-SMA gene has been shown to directly regulate the expression of α-SMA and fibroblast differentiation [41].

DNA methylation profiling studies have also shown a changed methylation pattern of CpG islands [42, 43].

The original hypothesis for the pathogenesis of IPF is that chronic inflammation causes alveolar epithelial cell injury, which leads to progressive fibrosis. There are several weaknesses with this theory. Inflammation is not a prominent histological finding, epithelial injury may stimulate fibrosis without inflammation, and anti-inflammatory therapy does not improve outcome of IPF [17, 44]. The new accepted hypothesis is that repetitive epithelial microinjuries result in abnormal activation of epithelial cells and aberrant wound healing, leading to the formation of the fibroblast/myofibroblast foci. These foci are frequently observed in IPF biopsy and correlated to survival [45, 46]. In the foci, myofibroblasts secrete excessive amounts of extracellular matrix (ECM) proteins, mainly fibrillar collagens. In this progressive abnormal lung remodeling, several neighboring scars, together with the disproportionate secretion of some enzymes can provoke the formation of the honeycomb cysts through mechanical forces [6].

1.2 Epithelia-to-mesenchymal transition and pulmonary fibrosis

Most tissues and organs development involves several conversions of epithelial cells to mesenchymal cells through the process of epithelial-to-mesenchymal transition (EMT) and the reversed mesenchymal-to-epithelial transition (MET) [47]. EMT is a process whereby epithelial cells undergo transition to a mesenchymal phenotype. During EMT, epithelial cells lose phenotypic features, such as apical-basal polarity and specialized cell-cell adhesions, and acquire mesenchymal cell properties such as increased cell mobility and invasive property [47, 48]. EMT is essential for the early stages of development of most tissues. During development, several rounds of EMT and MET are required. These sequential rounds are referred to as primary, secondary, and tertiary EMT [47]. Primary EMT enables the development of the mesoderm from the epithelium during gastrulation, which is necessary for the formation of organs such as the lung and heart. It also participates in the

delamination of neural crest cells from the dorsal neural tube [47]. Later on, early mesodermal cells will condense into transient epithelial structures, which undergo secondary EMT to generate mesenchymal cells that differentiate into specific cells [47]. The endothelial cells from the atrioventricular canal to form the endocardial cushion is an example of tertiary EMT [47, 49]. EMT is also required during wound healing as a physiological response [50, 51].

While EMT is an integral process during development, it also contributes to the progression of tumors and to fibrosis in fully developed organs. In cancer, tumor cells become more invasive after undergoing EMT, which facilitates the metastasis and progression of the tumor [52]. Studies have found that loss of epithelial markers such as E-cadherin, and expression of mesenchymal proteins such as vimentin correlates with poor prognosis [53]. The release of single cell through EMT is found during the invasion of adenocarcinoma [53]. Several studies have demonstrated that change of epithelial marker E-cadherin expression changes tumor invasive behavior [53, 54]. On the other hand, overexpression of twist, a TGF- β signaling pathway transcription factor, promotes EMT as well as the metastatic potential of tumor cells [55].

EMT not only occurs as a physiological response to injury, but it also occurs after tissue injury and/or stress and induces organ degeneration such as fibrosis. Many studies provide convincing evidence to support the hypothesis that a significant portion of the myofibroblasts in tissue fibrosis come from epithelial cells which have undergone EMT [47, 48, 53, 56-59]. Now we know cells of renal tubules, lens epitheliaum, hepatocytes all can undergo EMT [47]. Indeed, one study compared alveolar type II cells from fibrotic and normal human lungs. They found that cells from the lungs of patient with IPF had a higher expression of mesenchymal markers such as type I collagen. They also found that alveolar type II cells could acquire features of mesenchymal cells [60]. In vitro and in vivo studies suggest that alveolar epithelial cells can acquire mesenchymal characteristics in response to injury [56, 60-63].

Many signaling pathways are known to regulate EMT, including the TGF-β, Wnt and Notch pathways. These pathways do not operate independently; rather, crosstalk between them ensures EMT completion. The signaling pathway that conveys TGF-β inputs (TGFβ1) from membrane receptors to target genes is well studied, and is considered the central player in EMT. In lungs, TGFβ1 is synthesized and secreted, mainly by macrophages and epithelial cells, as a latent cytokine bound to latency-associated peptide (LAP) that both sequesters the cytokine's activity and localizes the cytokine to ECMs [64]. Activation of TGFβ1 in epithelial cells requires binding of latent TGFβ1 to integrin αvβ6 on epithelial cells, and then the activation of the integrin by G protein-coupled responses to proinflammatory agonists, such as thrombin or LPA2, further activate TGFβ1 [65-67]. Activation of TGF-β signaling pathway also requires loss of normal cell contacts, which triggers the assembly of signaling complexes that contain E-cadherin/β-catenin, integrin α3β1, and TGFβ1 receptors. The induced transcriptional complexes, tyrosine-phosphorylated β-catenin and phosphorylated Smads (p-Smads), move and accumulate in the nucleus to reprogram epithelial cells towards EMT [68].

1.3 Fibroblast differentiation and pulmonary fibrosis

Several possible origins for the IPF fibroblasts/myofibroblasts foci have been proposed, including resident fibroblasts, epithelial cells (via EMT), and bone marrow-derived cells (fibrocytes) [6]. Activated alveolar epithelial cells (AECs) secrete various mediators such as platelet-derived growth factor (PDGF), tumor necrosis factor α, TGFβ, and endothelin 1, which cause migration, proliferation and differentiation of resident fibroblasts [69]; AECs also have a high expression of chemokine CXCL12 and circulating fibrocytes express the chemokine receptor CXCR4, suggesting that fibrocytes are recruited through CXCR4-CXCL12 axis [70]; AECs may directly contribute to the fibroblasts/myofibroblasts population through the EMT [60, 62, 71].

Activated fibroblasts can differentiate into contractile and secretory myofibroblasts which cause excessive contraction and extracellular matrix (ECM) deposition. The hallmark of differentiated myofibroblasts is the expression of α-smooth muscle actin (α-SMA). At least three actors are required to induce fibroblast differentiation: local accumulation of active TGFβ1, high extracellular mechanical stress, and the presence of specialized ECM proteins [72]. Differentiated myofibroblasts exaggerate the ECM accumulation. They secrete angiotensinogen and hydrogen peroxide, which induce AEC apoptosis. They also produce matrix metalloproteinases, which disrupt the basement membrane [73, 74]. Fibroblasts and myofibroblasts in IPF are more resistant to apoptosis, causing persistent foci in the lung tissue [75].

1.4 TGF-β signaling pathway

The signaling pathway that conveys TGF-β inputs from membrane receptors to target genes is well studied. TGF-β binds trans-membrane serine–threonine kinase receptors on the cell surface, leading to the formation of a bi-dimeric receptor complex of receptor type I (TβRI) and type II (TβRII). TβRII phosphorylates and activates TβRI, which then phosphorylates cytoplasmic Smad2/3 transcription factors, allowing them to translocate into the nucleus. Smad4 acts as a partner with Smad2/3 to facilitate this process. In contrast, Smad6 and Smad7 inhibit the activated receptor-regulated Smad2/3. Three families of the transcription factors (Snail, ZEB and bHLH) are all involved in the TGF-β transcription program. Their expression is regulated either directly through a Smad-dependent pathway, or indirectly through other transcription factors. These transcription factors repress epithelial genes (e.g., E-cadherin and zonula occludens-1) and activate mesenchymal genes (e.g., N-cadherin and α-smooth muscle actin) [76]. Nuclear import of Smad3 requires a nuclear localization sequence (NLS) in the MH1 domain, which is exposed by phosphorylation, allowing its binding importin-β. Smad2 importing is independent of importin-β but requires MH2 domain. In the nucleus, phosphor-Smad2/3 are dephosphorylated by PPM1A and exported to the cytoplasm, which requires the interaction between MH2 domain and nucleoporins CAN/Nup214 and Nup153 [77].

Functionally, the TGF-β signaling pathway plays a predominant role in tissue fibrosis by influencing processes such as EMT, fibroblast recruitment, fibroblast contractility, myofibroblast differentiation, and ECM deposition [78-81].

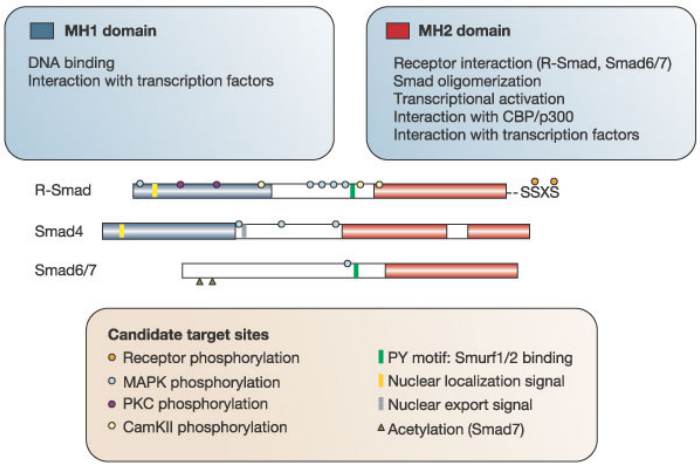

Fig. I.1. Structural organization and role of the domains of Smads [77].

1.5 microRNA in pulmonary fibrosis

MicroRNAs (miRNAs) are a group of small non-coding RNAs that are 18-24 nt in length and regulate gene expression at the post-transcriptional level. miRNAs are first transcribed from miRNA genes by RNA polymerase II, then cleaved by Drosha/Dicer to become mature miRNAs. The mature single-stranded miRNA is incorporated into the RNA-induced silencing complex (RISC), which binds to target mRNAs to inhibit protein translation or to cleave the mRNAs. miRNAs regulate both physiological and pathological processes [82-86].

A number of miRNAs have been reported to be involved in fibrotic diseases [86]. The miR-200 family and miR-205 target ZEB1 and SIP1, two important transcriptional factors in the TGF-β pathway, and inhibit EMT in renal epithelial cells [87, 88]. Recently, miR-424 has been shown to induce EMT in cancer cells [89]. Several other miRNAs are also implicated in fibrotic lung diseases. TGF-β1 induces miR-21 expression, and miR-21 in turn promotes activation of fibroblasts by

inhibiting Smad7 [90]. miR-155 targets the keratinocyte growth factor in lung fibroblasts to induce fibrosis [91]. Knock-down of miR-29 increases several pro-fibrotic genes in lung fetal fibroblasts [92]. A decrease in Let-7d is observed in the lungs of IPF patients, and studies in rat lung epithelial cells suggest that Let-7d contributes to EMT through its target, HMGA2 [88]. However, no direct evidence has been presented to show that miRNAs regulate EMT in human lung epithelial cells.

1.6 Enhancer of zeste homolog 2 (EZH2)

Enhancer of zeste homolog 2 (EZH2) is the catalytic component of a multiprotein complex, Polycomb Repressive Complexes 2 (PRC2) [183]. PRC2 catalyzes trimethylation of histone H3 lysine 27 (H3K27me3). EZH2 contains a SET domain which provides the methyltransferase active site, although EZH2 alone exhibits no intrinsic enzymatic activity. In order to attain catalytic activity it must be complexed with at least two proteins, embryonic ectoderm development (EED) and suppressor of zeste 12 (SUZ12) [93-95]. These three proteins combine with the histone binding proteins retinoblastoma binding protein 4 (RBBP4) and RBBP7 to form the core component of PRC2 [96]. Besides interacting with PRC2 components, EZH2 also interacts with other proteins including the transcription factor YinYang1 (YY1) [97, 98] and nuclear inhibitor of protein Ser/Thr phosphate-1 (NPP1) [99]. Over-expression of EZH2 has been associated with several cancers including prostate cancer, breast cancer, bladder cancer and lung cancer [100, 101]. Cigarette smoke induces EZH2 mediated repression of the Wnt signaling inhibitor Dickkopf-1 in lung cancer cells [102]. EZH2 is also the target of miR-101 and the genomic loss of miR-101 in cancer leads to over-expression of EZH2, resulting in cancer progression [103, 104].

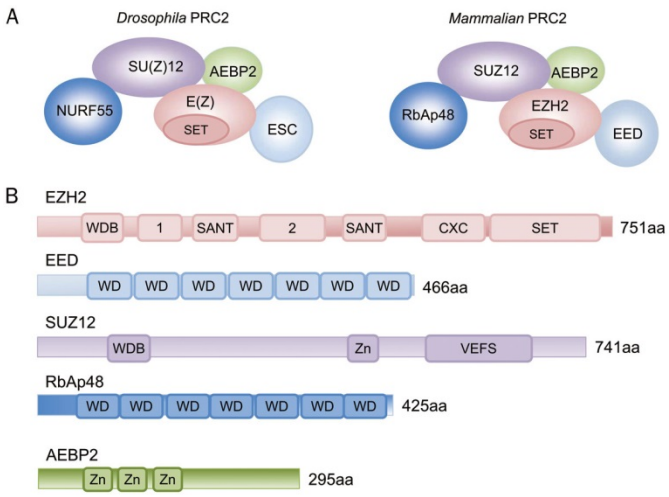

Fig.I.2. Architecture of PRC2 and its components [183]. (A) Models of PRC2. (B) Domain structure of components of PRC2. Domain "1", binding region for PHF; domain "2", binding region for SUZ12; CXC, cysteine-rich domain; SANT, domain that allows chromatin remodeling protein to interact with histones; SET, catalytic domain of EZH2;

1.7 Specific aims and significances

In spite of the great progress on the study of the pathogenesis of IPF, the exact cause is still unknown. IPF is still a disease with poor prognosis. EMT and fibroblast differentiation have been considered as two of the main players in this process, though there are still a lot of questions need to be answered. Thus, the present study is designed to better understand the molecular mechanism behind EMT, fibroblast differentiation of IPF. We have laid down two specific objectives:

Specific Aim I: Investigate the regulation of myofibroblast differentiation by miR-424 during epithelial-to-mesenchymal transition

Specific Aim II: Explore the role of EZH2 on myofibroblast differentiation in idiopathic pulmonary fibrosis

CHAPTER II

MATERIALS AND METHODS

2.1 Culture of human LL29 cells

Human lung fibroblasts (LL29, AnHa), isolated from a 26 years old female Caucasian, were purchased from the American Type Culture Collection (ATCC, Manassas, VA) and cultured in F-12K medium (Kaighn's Modification of Ham's F-12 Medium, ATCC), supplemented with 1% penicillin/streptomycin and 10% heat-inactivated fetal bovine serum (FBS). Cells were grown in cell culture flasks in a cell culture incubator at 37^{o}C in a humidified atmosphere containing 5% carbon dioxide. Culture medium was changed every 3 days.

2.2 Cell model of fibroblast activation and inhibition

LL29 cells were sub-cultured after reaching 100% confluence. The cells were trypsinized using 0.05% Trypsin-EDTA (Thermo Fisher Scientific, Grand Island, NY) and counted under a microscope. 1.6×105 cells per well were cultured in full F12-K culture medium in 12-well plates. After reaching 70% confluence, the cells were treated with 4 μM of 3-Deazaneplanocin A hydrochloride (DZNep, Sigma-Aldrich, St. Louis, MO) for 24 hours, followed by stimulation with 5 ng/ml of recombinant human TGF-β1 (R&D Systems, Minneapolis, MN) for another 24 hours. The cells were then washed with ice-cold phosphate-buffered saline (PBS, Thermo Fisher Scientific, Grand Island, NY) and collected either with Tri Reagent (Molecular Research Center,

Cincinnati, OH) for RNA isolation or M-PER Mammalian protein extraction reagent (Thermo Fisher Scientific, Grand Island, NY) plus Halt protease and phosphatase inhibitor cocktail (Thermo Fisher Scientific) for protein extraction. These samples were stored in – 80°C until use.

2.3 Culture of human A549 cells

Human lung epithelial cells (A549) were purchased from the American Type Culture Collection (ATCC, Manassas, VA) and cultured in Dulbecco's Modified Eagle's Medium (DMEM), supplemented with 1% penicillin/streptomycin and 10% heat-inactivated fetal bovine serum (FBS). Cells were grown at 37^{o}C in a humidified atmosphere containing 5% CO2. Cell model of EMT

A549 cells (1.6 x 105 per well) were cultured in DMEM, supplemented with 10% charcoal-stripped FBS in 6-well plates. After reaching 60% confluence, the cells were treated with 5 ng/ml of recombinant human TGF-β1 (R&D Systems, Minneapolis, MN) or with vehicle alone for 4, 8 and 12 days. The concentration of TGF-β1 used in our study (5 ng/ml) was based on the report from literature [107] and was physiologically relevant [108]. To avoid confluence, the cells were split every 4 days using trypsin. One third of the cells were reseeded in the original plates, while the other two thirds were collected for mRNA and protein analyses.

2.4 Human lung tissue

Twenty-eight lung tissue samples from IPF patients were obtained from Lung Tissue Research Consortium (LTRC). The tissues were divided into three groups according to the predicted probronchodialator forced vital capacity (FVC) of the patients: > 80% (n = 8), 50% - 80% (n = 10), and < 50% (n = 10). The lung tissues were stored in RNAlater solution -80°C until use.

2.5 Real-time PCR

Total RNA was isolated from cultured A549 LL29 cells, human or animal lung tissues using TRI Reagent following the manufacturer's instructions. Briefly, the samples in Tri Reagent were homogenized and waited for 5 minutes at room temperature to allow the complete dissociation of nucleoprotein complexes. Then, 0.1 ml 1-bromo-3-chloropropane (BCP) was added to 1 ml of the homogenate. The samples were mixed vigorously for 15 seconds, incubated at room temperature for 10 minutes, and centrifuge at 12,000 g for 15 minutes at 4°C. The upper aqueous phase was transferred to a new tube and mixed with 0.5 ml of isopropanol. The mixture was incubated at room temperature for 10 minutes and centrifuge at 12,000 g for 8 minutes at 4°C. The supernatant was removed. The white RNA pellet was washed with 75% ethanol, and centrifuged at 7,500 g for 5 minutes at 4°C. The RNA pellet was air-dried for 5 minutes and dissolved in RNase- and DNase-free distilled water. The RNA concentration and quality was determined using NanoDrop ND-1000 Spectrophotometer (NanoDrop Tech., Rockland, DE). The A260/A280 and A260/A230 of the RNA samples were greater than 1.8 and 1.7, respectively. Two µg of RNA was treated with TURBO DNase (Ambion, Austin, TX) in a 50 µl reaction buffer to remove genomic DNA contamination. The DNase was inactivated by performing a phenol/chloroform extraction. One µg of RNA was reverse-transcribed into cDNA using M-MLV reverse transcriptase, random primers, and oligo dT (all from Promega, Madison, WI). cDNA was diluted to 1:100 for real-time PCR of all mRNAs and 1:1,000 for 18S rRNA housekeeping gene. Real-time PCR was carried out on a 7900HT Fast Real-Time PCR System (Applied Biosystems, Foster City, CA) using 7500 software V2.3. The primers were designed using Primer Express software (Applied Biosystems) . Primers for miR-424 study are listed in Table II.1, and primers for EZH2 study are listed in Table II.2. The reaction system was 20 µl consisted of one µl each of 10 mM of forward and reward primers, 3 µl of water, 10 µl of qPCR Mastermix Plus for SYBR Green I – Low ROX (AnaSpec, Fremont, CA), and 5 µl of diluted cDNA. The thermal condition

was 95°C for 10 min, followed by 40 cycles of 95°C 15 s, and 60°C for 60 s. The mRNA levels of each gene were calculated using comparative CT (ΔΔCT) method. ΔCT was first calculated as mRNA CT minus housekeeping gene CT and then converted to the linear form of relative expression by the 2^(-ΔCT) calculation.

Real-time PCR for miRNAs was carried out as previously described [109, 110]. Briefly, two µg of total RNA, without DNase treatment, was polyadenylated using a Poly(A) polymerase tailing kit (Epicentre, Madison, WI). One µg of the poly(A) tailed RNA was then reverse-transcribed into cDNA using M-MLV reverse transcriptase, oligo dT and miRNA RT primers, including a universal reverse primer and a specific forward primer for each target miRNA listed in Table 2. Real-time PCR was performed using miRNA PCR primers (Table II.3). Data were normalized to RNU6B small RNA.

Table II.1: Real-time PCR primers for human mRNAs in miR-424 study

CDH1 Forward	5’ TGCCCAGAAAATGAAAAAGG
CDH1 Reward	5’ GTGTATGTGGCAATGCGTTC
CDH2 Forward	5’ CTGCACAGATGTGGACAGGATT
CDH2 Reward	5’ TTCTTTATCCCGGCGTTTCAT
α-SMA Forward	5’ GAGAAGAGTTACGAGTTGCCTGA
α-SMA Reward	5’ TGTTAGCATAGAGGTCCTTCCTG
ZEB1 Forward	5’ AGCAGTGAAAGAGAAGGGAATGC
ZEB1 Reward	5’ GGTCCTCTTCAGGTGCCTCAG
SIP1 Forward	5’ CCACCACCTACAAGCTCACTCC
SIP1 Reward	5’ AATGGCGATGGCGAGGAGAC
E2A Forward	5’ TGTGCCAACTGCACCTCAA
E2A Reward	5’ CCGTTTCAAACAGGCTGCTT
Id2 Forward	5’ CGTGAGGTCCGTTAGGAAAA
Id2 Reward	5’ AGGCTGACAATAGTGGGATG
Id3 Forward	5’ ACTCACTCCCCAGCATGAAG
Id3 Reward	5’ AAGCTCCTTTTGTCGTTGGA
Snail1 Forward	5’ AGGATCTCCAGGCTCGAAAG
Snall1 Reward	5’ GTAGCAGCCAGGGCCTAGAG
Snail2 Forward	5’ CTGCGGCAAGGCGTTTTCCAGA
Snail2 Reward	5’ CAGATGAGCCCTCAGATTTGAC
Twist Forward	5’ CGGACAAGCTGAGCAAGATT
Twist Reward	5’ CCTTCTCTGGAAACAATGAC
CTGF Forward	5’ CAGCATGGACGTTCGTCTG
CTGF Reward	5’ AACCACGGTTTGGTCCTTGG
FN Forward	5’ AGCCTCGAAGAGCAAGAGG
FN Reward	5’ CAAAACTTCAGCCCCAACTT
Smurf1 Forward	5’ AGATCCGTCTGACAGTGTTATGT
Smurf1 Reward	5’ AGATCCGTCTGACAGTGTTATGT
Smurf2 Forward	5’ GGCAATGCCATTCTACAGATACT
Smurf2 Reward	5’ CCACTTTGGATCAAGCGTATTCT
Smad7 Forward	5’ ATAGCTAGCGCTTTACCGTGCAGATCAGCTT
Smad7 Reward	5’ ATAGTCGACTTAATGGAACATAAACTCCTTT
18S rRNA Forward	5’ CGTTGATTAAGTCCCTGCCCTT
18S rRNA Reward	5’ TCAAGTTCGACCGTCTTCTCAG

Table II.2. Real-time PCR primers in EZH2 study

Human-EZH2-FW	TCCTACATCCTTTTCATGCAACAC
Human-EZH2-RE	CCCTCCAAATGCTGGTAACAC
Mouse-EZH2-FW	TGTGACCCTGACCTCTGTCTCA
Mouse-EZH2-RE	AGACGGTGCCAGCAGTAAGTG
Human-18S-FW	CGTTGATTAAGTCCCTGCCCTT
Human-18S-RE	TCAAGTTCGACCGTCTTCTCAG
Mouse-18S-FW	ATTGCTCAATCTCGGGTGGCTG
Mouse-18S-RE	CGTTCTTAGTTGGTGGAGCGATTTG
Human-GAPDH-FW	GAAGGTGAAGGTCGGAGTCAAC
Human-GAPDH-RE	CATGGGTGGAATCATATTGGAA
Human-ACTB-FW	GGCACCACACCTTCTACAATGA
Human-ACTB-RE	ACAGCCTGGATAGCAACGTACA
Mouse-GAPDH-FW	CTCGTCCCGTAGACAAAATGGT
Mouse-GAPDH-RE	TGATGGCAACAATCTCCACTTT
Mouse-ACTB-FW	GGCCAACCGTGAAAAGATGA
Mouse-ACTB-RE	TCCATCACAATGCCTGTGGTA
Human-αSMA-FW	GTGTTGCCCCTGAAGAGCAT
Human-αSMA-RE	CGCCTGGATAGCCACATACAT
Mouse-αSMA-FW	ATCCGATAGAACACGGCATCA
Mouse-αSMA-RE	CAGCAGTGTCGGATGCTCTTC
Human-Fibronectin-FW	CCTGCATCTGAGTACACCGTATC
Human-Fibronectin-RE	GGTCTCAGTCACCTCGGTGTT
Human-COL4A1-FW	CTCTGGCTGTGGCAAATGTG
Human-COL4A1-RE	CCTCAGGTCCTTGCATTCCA
Mouse-COL1A1-FW	ACGCATGGCCAAGAAGACAT
Mouse-COL1A1-RE	TTGTGGCAGATACAGATCAAGCA
Mouse-COL3A1-FW	CACCCTTCTTCATCCCACTCTT
Mouse-COL3A1-RE	TGACATGGTTCTGGCTTCCA

Table II.3: Primers for miRNA Reverse transcription and real-time PCR

Reverse transcription Primers	
has-miR-Universe	GTCGTGTCCAGTCGTGTGTT
hsa-miR-1183	GCGAGCACAGAATTAATACGACTCACTATAGG(T)12GCCCA
hsa-miR-23b-5p	GCGAGCACAGAATTAATACGACTCACTATAGG(T)12AAATCA
hsa-miR-1224-3p	GCGAGCACAGAATTAATACGACTCACTATAGG(T)12CTGAGG
hsa-miR-155	GCGAGCACAGAATTAATACGACTCACTA TAGG(T)12ACCCCT
hsa-miR-298	GCGAGCACAGAATTAATACGACTCACTATAGG(T)12GGGAG
hsa-miR-933	GCGAGCACAGAATTAATACGACTCACTATAGG(T)12GGGAGA
hsa-miR-31	GCGAGCACAGAATTAATACGACTCACTATAGG(T)12AGCTAT
hsa-miR-424	GCGAGCACAGAATTAATACGACTCACTATAGG(T)12CAAA
hsa-miR-216b	GCGAGCACAGAATTAATACGACTCACTATAGG(T)12CACAT
hsa-miR-219-2-3p	GCGAGCACAGAATTAATACGACTCACTATAGG(T)12ACAGCT
hsa-miR-190	GCGAGCACAGAATTAATACGACTCACTATAGG(T)12ACCTAA
hsa-miR-1273	GCGAGCACAGAATTAATACGACTCACTATAGG(T)12AAGAAA
hsa-miR-582-5p	GCGAGCACAGAATTAATACGACTCACTATAGG(T)12AGTAAC
hsa-miR-487a	GCGAGCACAGAATTAATACGACTCACTATAGG(T)12AACTGG
hsa-miR-136-3p	GCGAGCACAGAATTAATACGACTCACTATAGG(T)12AGACTC
Real-time PCR primers	
hsa-miR-1183	ACTGACCACTGTAGGTGATGGT
hsa-miR-23b-5p	CAATTATGGGTTCCTGGCATGC
hsa-miR-1224-3p	ATTAATCCCCACCTCCTCTCTC
hsa-miR-155	GCCGGCTTAATGCTAATCGTGA
hsa-miR-298	TACATAGCAGAAGCAGGGAGG
hsa-miR-933	ATTATATGTGCGCAGGGAGACC
hsa-miR-31	AGTCGTAGGCAAGATGCTGGC
hsa-miR-424	GCTCGACAGCAGCAATTCATGT
hsa-miR-216b	CGAGCTAAATCTCTGCAGGCAA
hsa-miR-219-2-3p	CTGCATAGAATTGTGGCTGGAC
hsa-miR-190	CCGCGCTGATATGTTTGATATA
hsa-miR-1273	TCTAGTGGGCGACAAAGCAAGA
hsa-miR-582-5p	CGACGGTTACAGTTGTTCAACC
hsa-miR-487a	CGTGCGAATCATACAGGGACAT
hsa-miR-136-3p	GCTCGGCATCATCGTCTCAAAT

2.6 miRNA over-expression

These studies utilized lentiviral miRNA expression vectors containing three elements, CMV-driven EGFP, followed by the mature miRNA sequence plus flanking sequences, which were then followed by the SV40 PolyA terminal sequence. The mature miRNA sequence and its 5' and 3' flanking sequences of approximately 250 nt were PCR-amplified from human genomic DNA and cloned into the pLVX (Lenti-X) vector (Clontech, Mountain View, CA). The lentivirus was generated in HEK 293T cells using Lenti-X HTX packaging mix (Clontech). To determine the titer of viruses, different dilutions of viral stocks were used to infect 293T cells, followed by counting GFP-positive infected cells. A549 cells were infected with miRNAs or control lentivirus at MOI=50 for 24 h. After infection, virus-containing medium was removed and the cells were cultured for an additional 24 h in fresh medium.

2.7 TGF-β reporter luciferase assay

Four million HEK 293T cells were seeded on a 96-well plate. Fifty ng of a TGF-β reporter plasmid (SABiosciences, Valencia, CA), which contained a Smad transcriptional response element and a firefly luciferase reporter gene, and 100 ng of miR-424 lentiviral expression plasmid were co-transfected into HEK 293T cells using Lipofectamine 1000. A lentiviral plasmid containing a scrambled sequence was used as a control. After 24 h of incubation, the cells were treated with TGF-β1 (5 ng/ml) or vehicle for 24 h and assayed using the Dual-Luciferase Reporter Assay System (Promega, Madison, WI).

2.8 3'-UTR pmirGLO vector construction

3'-UTR segments of three predicted targets, Smad7, Smurf1 and Smurf2 of miR-424, containing restriction sites NheI and SalI on the 5' and 3' ends, were amplified using PCR. Three PCR products and the pmirGLO empty vector (Promega, Madison, WI) were double-digested

using NheI and SalI restriction endonucleases (New England Biolabs, Ipswich, MA). The 3'-UTR segments were then inserted into the pmirGLO vector using T4 DNA ligase (New England Biolabs, Ipswich, MA). The inserts were confirmed by sequencing.

2.9 Western blotting

The cells were directly lysed in M-PER mammalian protein extraction lysis buffer (PIERCE, Rockford, IL) for 30 minutes on a rocker at 4°C whereas the tissue samples were homogenized in the lysis buffer. The lysate was centrifuged at 12,000 rpm for 15 minutes at 4°C. The supernatant was transferred to a tube and stored at -80°C. Protein concentration was determined using DC protein assay (Bio-Rad, Hercules, CA). Ten to twenty µg of proteins were mixed with 6X SDS protein loading buffer and water to a total volume of ten to twenty-five ml. Samples were separated on SDS–PAGE gel using Mini Trans-Blot system (Bio-Rad, Hercules, CA) at a constant voltage of 300 mV, and then were transferred to a nitrocellulose membrane using Semi-wet Trans-Blot turbo transfer system at a constant currant of 1.5 mA. The membranes were blocked with 10% non-fat milk for 60 minutes at room temperature, and then incubated overnight at 4°C with primary antibodies (See Table 2 for sources and dilutions). The membrane was washed using Tris-Buffered Saline with Tween 20 (TTBS) and incubated with goat anti-mouse or goat anti-rabbit secondary antibodies (1:10000, Jackson ImmunoResearch, West Grove, PA) for 1 hour. The blots were then developed with enhanced chemiluminescence (ECL) reagents (PIERCE, Rockford, IL). Amersham Imager 600 (GE Healthcare Bio-Sciences, Pittsburgh, PA) was used to capture the images.

2.10 Gel contraction assay

The cells were trypsinized using trypsin EDTA and counted. Then the cells were mixed with collagen type 1 solution (BD Biosciences, San Jose, CA) with a final concentration of 1 x105 cells/ml and 1 mg/ml of collagen. Fifteen µl of 0.5 N NaOH per 1 ml of the mixture were

added. An aliquot of five hundred µl of the mixture was distributed to each well of 12-well plates immediately and the plates were incubated in cell culture incubator for 30 minutes for polymerization. The polymerized gel was detached from the well wall and bottom using a 200 µl pipette tip and 500 µl of full growth medium with or without DZNep or TGFβ1 was added to each well. The plates were then returned to the incubator with 5% CO2 and 95% air. Photos of each well were taken after 48 hours. By using Image J software, surface areas of gel and well bottom were measured. Gel contraction activity was expressed as the ratio of gel to well bottom surface area.

2.11 Nuclear and cytoplasmic extraction

Nuclear and cytoplasmic fractions were separated using NE-PER nuclear and cytoplasmic extraction reagents (Thermo Fisher, Grand Island, NY). LL29 cells were harvested using trypsin-EDTA and then centrifuged at 500 xg for 5 minutes. Cell pellet was washed with PBS and centrifuged at 500 x g for 3 minutes. The supernatant was removed, leaving the cell pellet as dry as possible. One hundred µl of CER I reagent with proteinase inhibitor was added to the tube. Cells were fully suspended by vigorously vortexing and incubated on ice for 10 minutes. CER II (5.5 µl) was then added. Tubes were vortexed for 5 seconds and centrifuged at 20,000 xg for 5 minutes. The supernatant (cytoplasmic extract) was transferred to a new tube and stored at -80°C. The remaining pellet was suspended in 50 µl of NER reagent with proteinase inhibitor. The tubes were vortexed vigorously for 15 minutes and placed on ice and continued vortexed for 15 seconds every 10 minutes, for a total of 40 minutes. The tubes were then centrifuged at 20,000 x g for 10 minutes, and the supernatant (nuclear extract) was transferred to a new tube and stored at -80°C for western blotting analysis.

2.12 Immunohistochemistry

Lung tissue sections were deparaffinized in xylene twice for 1 minute, and were hydrated in 100%, 95% and 70% alcohol and deionized water successively. Endogenous peroxidase activity was quenched using 0.3% H2O2 in water for 30 minutes at room temperature. The slides were blocked with 1.5% goat serum in PBS for 20 minutes at room temperature. The slides were then incubated for 60 minutes at room temperature with rabbit anti-EZH2 monoclonal antibodies (1:200 dilution, Cell Signaling Technology, Danvers, MA) in 1.5% goat serum in PBS. After being washed with PBS for 5 minutes, the slides were incubated with goat anti-rabbit biotinylated secondary antibodies (1:200 dilution) at room temperature for 30 minutes. Then the slides were incubated with ABC staining reagent (VECTASTAIN, Burlingame, CA) for 30 minutes. After the slides were washed in PBS for 5 minutes, they were incubated in peroxidase substrate to develop a desired color.

For EZH2 and α-SMA double-staining, the procedure for EZH2 ABC staining was the same as described above. Following anti-EZH2 antibodies incubation, tissue sections were incubated with anti-α-SMA antibodies (1:200 dilution) overnight at 4°C together with anti-EZH2 antibodies. ABC staining was performed for detecting EZH2, followed by incubation with Alexa Fluor 488 rabbit IgG fluorescent secondary antibody (1:3000, Life technologies, Grand Island, NY) for detecting α-SMA. Images were taken for bright field and fluorescence in the same field.

2.13 Primary Mouse Fibroblasts/Myofibroblasts Isolation

Fibroblasts and myofibroblasts were isolated from ten-week old of female C57BL/6 mice with or without bleomycin challenge according to the previous studies [113, 114]. The lungs were first trimmed to remove major airways and rinsed with PBS. Lung tissue then was transferred into 100 mm cell culture dishes and minced into 1 to 2-mm3 pieces. Minced lung was incubated with 5 ml of 0.25% Trypsin-EDTA (Thermo Fisher Scientific, Grand Island, NY) in cell culture

incubator at 37°C. At each of three 10-minute intervals, dishes were gently shaken by hand. After 30 minutes, the cells were centrifuged at 1,200 rpm at 4°C for 10 minutes. The pellet was suspended in 10 ml of Dulbecco's modified Eagle's medium (DMEM) supplemented with 10% fetal bovine serum, and transferred into 100 mm dishes. After 1 week of culture in the incubator at 37°C, nonadherent cells were removed while adherent cells were trypsinized and passed through 70 μm sterile cell strainers (Thermo Fisher Scientific, Grand Island, NY). The passed-through fibroblasts/myofibroblasts were cultured in DMEM with 10% FBS until grown to 100% confluency, and then were stored in liquid nitrogen for further use.

2.14 Construction of shRNA vector

We used BLOCK-iT RNAi Designer, an online software from Thermofisher.com to design oligonucleotides for EZH2 shRNAs, The highest ranked target sequence, GCAGCTTTCTGTTCAACTTGA, was chosen. For the forward (FW) oligo, GATCC, a sequence for BamH1 restriction enzyme was added to the 5' of the target sequence. TTCAAGAGA, a loop sequence, was added to the 3' followed by antisense sequence. TTTTTG was added to the 3' end of the oligo. The final sequence was GATCCGCAGCTTTCTGTTCAACTTGATTCAAGAGATCAAGTTGAACAGAAAGCTGTTTTTG. For the reverse (RE) oligo, AATTCAAAA, a sequence for EcoR1 restriction enzyme was added to the 5' of the target sequence. Loop sequence, TCTCTTGAA, was added between the target sequence and the antisense sequence. Another G was added to the 3' end. The final sequence was AATTCAAAAAGCAGCTTTCTGTTCAACTTGATCTCTTGAATCAAGTTGAACAGAAAGCTGG. FW and RW oligo was annealed in annealing buffer (Promega, Madison, WI).

pGreenPuro vector (System Biosciences, Mountain View, CA) was first double-digested using BamH1 and EcoR1 restriction enzymes. The annealed oligo then was ligated with the

digested pGreenPuro vector using T4 ligase (Promega, Madison, WI). The plasmids were transformed and amplified in competent cells (E. Coli ST3). The final plasmids were isolated using the QIAprep Spin Miniprep Kit (Qiagen, Valencia, CA). The sequence of the insert was confirmed by sequencing.

2.15 Preparation of lentivirus and titer determination

HEK293T cells were seeded in 100 mm cell culture dishes and cultured in 37°C incubator with 5% CO2 and 95% air overnight. The medium was replaced with 9 ml of Opti-mem medium containing 4% fetal bovine serum (FBS). The culture dishes were put back to an incubator. Meanwhile, 1.5 ml of Opti-mem medium was gently mixed with 3 µg of shRNA/control plasmid and 9 µg of Lenti-X HTX packaging mix (Clontech, Mountain View, CA). Another 1.5 ml of Opti-mem was gently mixed with 36 µl of Lipofectamine 2000 (Thermo Fisher Scientific, Grand Island, NY). After incubating at room temperature for 5 minutes, the two mixtures were mixed and incubated for 20 minutes at room temperature. 3 ml of the final mixture wad added into each dish and cultured overnight. The medium was then replaced with full growth medium (DMEM with 10% of FBS and 1% of penicillin-streptomycin). After 24 hours, the medium containing lentiviruses was centrifuged at 1,000 g for 15 minutes at 4°C, aliquoted into 1 ml per tube, and stored at -80°C until use.

To determine the lentivirus titer, 1 ml of HEK293T cells (5×10^5 cells/ml) was seeded in each well of 12-well plates and cultured for 24 hours. 500 µl of 1,000 times diluted in full growth medium were added into each well, and incubated for 24 hours. Green fluorescent protein (GFP) positive cells were counted under a 20X objective using a fluorescent microscope for ten random fields. The titer was calculated as mean (GFP positive cells) x 594 (fields)/0.5 ml x 10-3 (IU/ml).

2.16 Infection of cells with shRNA lentivirus

1 x 10^5 of LL29 cells were seeded in each well of 12-well plates and cultured overnight in 1 ml of full growth medium in an incubator. The lentiviruses were then added at a multiplicity of infection (MOI) of 100. Polybrene (1:200) was also added into the medium to increase the efficiency of infection. 24 hours after infection, the virus medium was replaced with full growth medium. After another 24 hours, cells were treated with 5 ng/ml of TGFβ1 for 24 hours.

2.17 Co-Immunoprecipitation (Co-IP)

LL29 cells were treated with DZNep for 48 hours and stimulated with 5 ng/ml of TGFβ1 for 60 minutes. The cells were lysed using M-PER mammalian protein extraction lysis buffer for 30 minutes on a rocker at 4°C. The lysate was centrifuged at 12,000 rpm for 15 minutes at 4°C. The supernatant was transferred to a tube and stored at -80°C. Protein concentration was determined using DC protein assay. 220 µg of cell lysate was taken to a fresh tube, and made to a total volume of 220 µl using lysis buffer. 200 µl of the lysate was transferred to fresh tubes and was incubated on ice with anti-EZH2 antibodies (1:50) for one hour on ice. 20 µl of protein A/G beads was added into the lysate. The mixture was rotated at 4°C overnight and centrifuged at 10,000 rpm for 7 minutes at 4°C. The supernatant was transferred to fresh tubes and saved as "out" fraction. The remaining pellet (beads) was washed with 1 ml of PBS for 4 times. 80 µl of 1X protein loading buffer were added and boiled for 7 minutes. 20 µl of each sample were taken for western blotting using anti-EZH2 and anti-Smad2/3 antibodies.

2.18 Phosphorylation of Smad2/3

LL29 cells were treated with DZNep for 48 hours, and then with 5 ng/ml of TGFβ1 for 0, 30, 60 and 120 minutes. Cells were lysed using M-PER mammalian protein extraction lysis buffer with proteinase and phosphatase inhibitors (1:100) for 30 minutes on a rocker at 4°C. The lysate

was centrifuged at 12,000 rpm for 15 minutes at 4°C. The supernatant was transferred to a tube and stored at -80°C until use. Protein concentration was determined using DC protein assay. Western blotting was performed using anti-phospho-Smad2/3 primary antibodies and total Smad2/3 antibodies.

2.19 Mouse model of pulmonary fibrosis

Ten-week old female C57BL/6 mice (The Jackson Laboratory, Bar Harbor, ME) were housed in the Animal Resources at Center for Veterinary Health Sciences, Oklahoma State University. The animal procedures were approved by the Institutional Animal Care and Use Committee (IACUC) at the Oklahoma State University. Mice were anesthetized using Ketamine and Xylazine mixture through intraperitoneal injection. The mice were then challenged with 50 µl of PBS or 1 unit/kg of bleomycin (Sigma-Aldrich, St. Louis, MO) in 50 µl PBS through an intratracheal route. EZH2 inhibitor DZNep (2 mg/kg) in 300 µl PBS was given every day through intraperitoneal route beginning 1 day before bleomycin instillation until day 17. Lung tissues were collected on day 17 after bleomycin challenge. The right lung was fixed with 4% formaldehyde for H&E staining and immunostaining. The left lung was minced, and then grounded into powder in liquid nitrogen, half of the sample was homogenized using Tri Reagent for real-time PCR and another half was homogenized using M-PER protein lysis buffer for Western blotting. The severity of pulmonary fibrosis was evaluated by Ashcroft scores according to the method of Ashcroft [115].

2.20 Statistical analysis

Statistical analyses were performed using Student's t-test for two independent groups and one-way ANOVA, followed by Tukey's post hoc test or two-way ANOVA, followed by Bonferroni's post hoc test for multiple comparisons. $P < 0.05$ was considered significant.

CHAPTER III

RESULTS

3.1 miR-424 induces myofibroblast differentiation during Epithelial-to-Mesenchymal Transition

3.1.1 TGF-β1 reduces epithelial cell marker expression and increases mesenchymal cell marker expression

In order to investigate the role of miRNAs in EMT, we used a TGF-β1-induced EMT cell model [107]. We treated human lung epithelial A549 cells with 5 ng/ml of TGF-β1 for 4, 8, or 12 days, and determined epithelial and mesenchymal cell mRNA marker expression. E-cadherin (CDH1), an epithelial marker, was down-regulated in a time-dependent manner. It dramatically decreased on day 4 and was barely detectable on day 12 (Fig. III.1.1A). N-cadherin (CDH2), a mesenchymal marker, was increased on day 4, peaked on day 8 and returned to the day 4 level by day 12 (Fig. III.1.1B). α-smooth muscle actin (α-SMA), a myofibroblast marker, was marginally increased on day 8 (Fig. III.1.1C), consistent with a previous report [107]. These results indicate that TGF-β causes EMT, but is not sufficient for myofibroblast differentiation.

We further examined genes that encode key transcription factors in the TGF-β signaling pathway. We found that mRNA for ZEB1, a repressor of epithelial genes, peaked on Day 8 (Fig. III.1.2A). However, SIP1, another repressor of epithelial genes, was not significantly affected at

any time point by TGF-β (Fig. III.1.2B). Among other transcription factors in the TGF-β signaling pathway which were tested, Snail2 mRNA showed the greatest increase by TGFβ, while Id2 (an inhibitor of the E-cadherin repressor, E2A) showed the greatest decrease (Fig. III.1.2C).

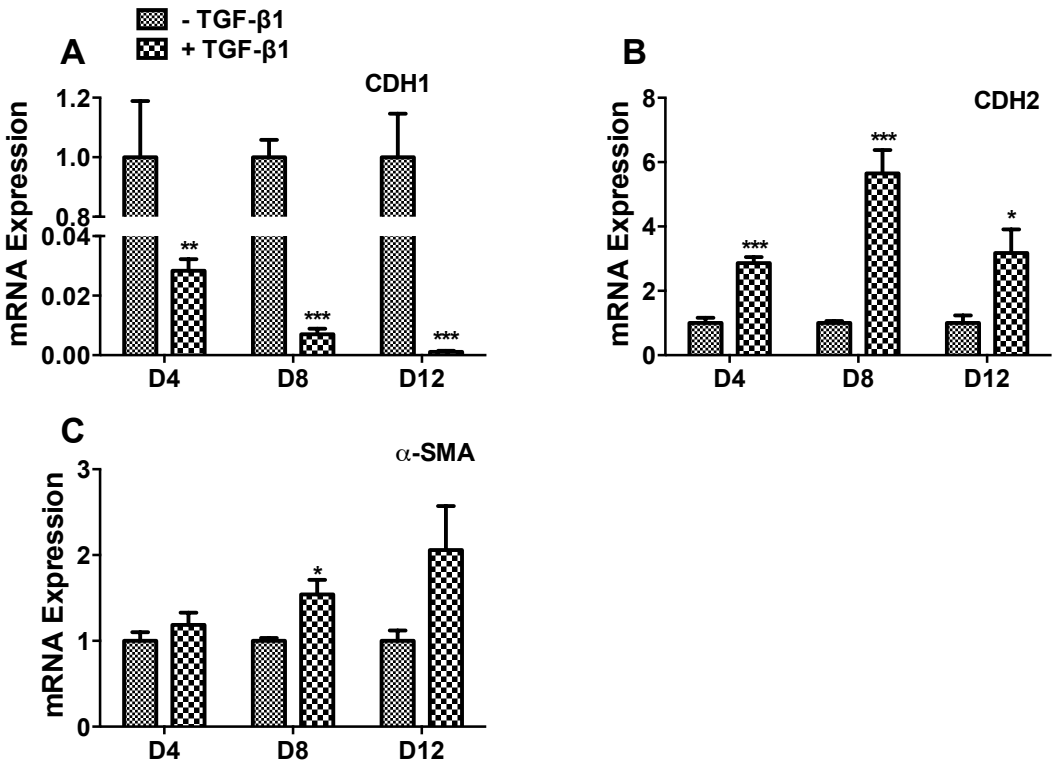

Fig. III.1.1. TGF-β1 induces EMT in human alveolar epithelial cells. Human A549 cells were treated with TGF-β1 (5 ng/ml) for 4, 8 and 12 days (D4, D8 and D12). The mRNA expressions of the cell markers were determined by real-time PCR. (A) Epithelial cell marker, E-cadherin (CDH1). (B) Mesenchymal cell marker, N-cadherin (CDH2). (C) Myofibroblast marker, α-smooth muscle actin (α-SMA). Results were normalized to 18S rRNA and expressed as a ratio of the TGF-β1 treated group to the control group at each time point. Results are means ± s.e. from the three independent experiments, which were performed in triplicate. *P<0.05 v.s. without TGF-β1; **P<0.01 v.s. without TGF-β1; ***P<0.001 v.s. without the TGF-β1. Student's t-test.

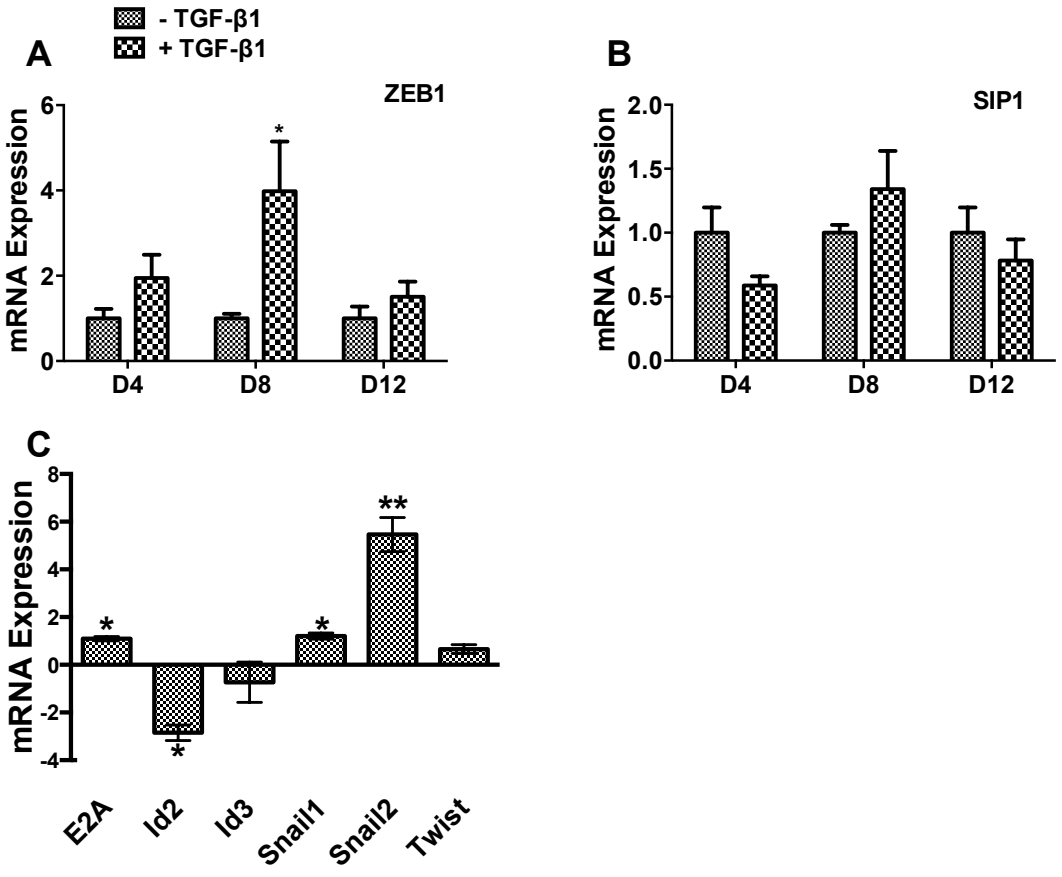

Fig. III.1.2. Effects of TGF-β on transcription factors. A549 cells were treated with TGF-β1 (5 ng/ml) for 4, 8 and 12 days (D4, D8 and D12). The mRNA levels of ZEB1 (A) and SIP1 (B) were measured by real-time PCR and expressed as a ratio of the TGF-β1 treated group to the control group at each time point. The mRNA levels of E2A, Id2, ID3, Snail1, Snail2, and Twist on day 8 after TGF-β1 were also determined by real-time PCR and expressed as delta delta C_T (C). Data were normalized to 18S rRNA. Results are means ± s.e. from the three independent experiments, which were performed in triplicate. *P<0.05 v.s. without TGF-β1; **P<0.05 v.s. without TGF-β1. Student's t-test.

3.1.2 Six miRNAs are up-regulated and three miRNAs are down-regulated during EMT

Since the mesenchymal cell marker, CDH2, and the transcription factor, ZEB1, peaked on day 8 of TGF-β1 treatment, we chose this time point for miRNA microarray analysis as

described in our previous studies [111, 112, 116], with a goal of identifying miRNAs involved in the process of EMT. We used in-house printed miRNA microarray slides containing 1,700 miRCURY LNA probes for human, rat and mouse miRNAs (EXIQON). After quality control and statistical analysis, six miRNAs were found to be up-regulated, while nine miRNAs were down-regulated. Since miRNA microarray is semi-quantitative [82], we used real-time PCR to verify the miRNA microarray data. We verified 9 miRNAs, including 6 up-regulated (miR-31, miR-190, miR-424, miR-136-3p, miR-487a and miR-582-5p) and 3 down-regulated (miR-1224-3p, miR-23b-5p and miR-933) miRNAs (Fig. III.1.3).

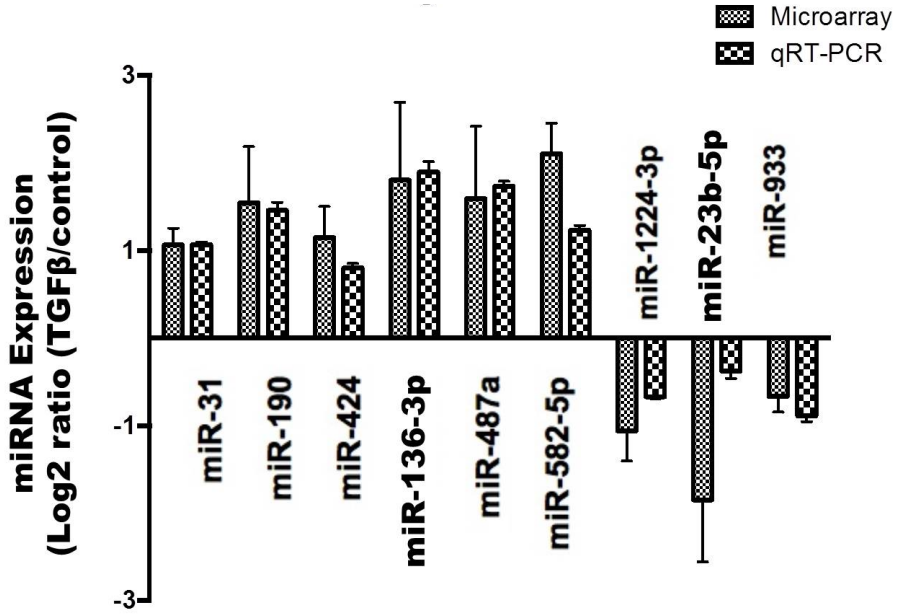

Fig. III.1.3 miRNAs changed during EMT. A549 cells were treated with 5 ng/ml of TGF-β1 for 8 days. miRNA microarray and real-time PCR were performed to identify the miRNAs changed during EMT. All real-time PCR data were normalized to RNU6B small RNA. The results were expressed as log2 ratio (TGF-β1-treated vs control). Data shown are means ± s.e. All microarray and real-time PCR results were statistically significant ($P<0.05$). n=3 cell preparations. Student's t-test.

3.1.3 Over-expression of miR-424 promotes myofibroblast differentiation

We designed two experiments to test whether the identified 9 miRNAs affected EMT. If TGF-β1-mediated EMT is due to the down-regulation of inhibitory miRNAs, the over-expression of these down-regulated miRNAs should inhibit TGF-β1-induced EMT. On the other hand, if the up-regulated miRNAs during EMT cause EMT, the over-expression of these miRNAs should mimic the effect of TGF-β1 treatment. We over-expressed the 3 down-regulated miRNAs in A549 cells using lentiviral miRNA expression vectors, treated the cells with TGF-β1, and determined the epithelial and mesenschymal cell marker expression. Real-time PCR analysis revealed that over-expression of those miRNAs had no effect on the expression of the epithelial marker CDH1 (Fig. III.1.4A) compared to the virus control. However, expression of the mesenchymal marker CDH2 was increased by 2 of the 3 miRNAs tested (miR-1224-5p and miR-23b), which was an effect opposite to that expected if these miRNAs have a role in EMT (Fig. III.1.4B). Furthermore, miR-23b and miR-933 also slightly increased α-SMA expression (Fig. III. 1.4C). These results suggest that the 3 down-regulated miRNAs tested are likely not involved in EMT.

Next, we overexpressed the 6 up-regulated miRNAs in A549 cells without TGF-β1 treatment to see whether they could induce EMT. miR-136, miR-190, miR-31 and miR-424 had no effect on either the CDH1 or CDH2 expression (Fig. III. 1.4D, E). In contrast, miR-487a and miR-582 increased both epithelial (CDH1) and mesenchymal (CDH2) marker expression. This is not consistent with EMT, in which epithelial cell markers are decreased and mesenchymal cell markers are increased. However, miR-424 significantly increased α-SMA expression (Fig. III. 1.4F).

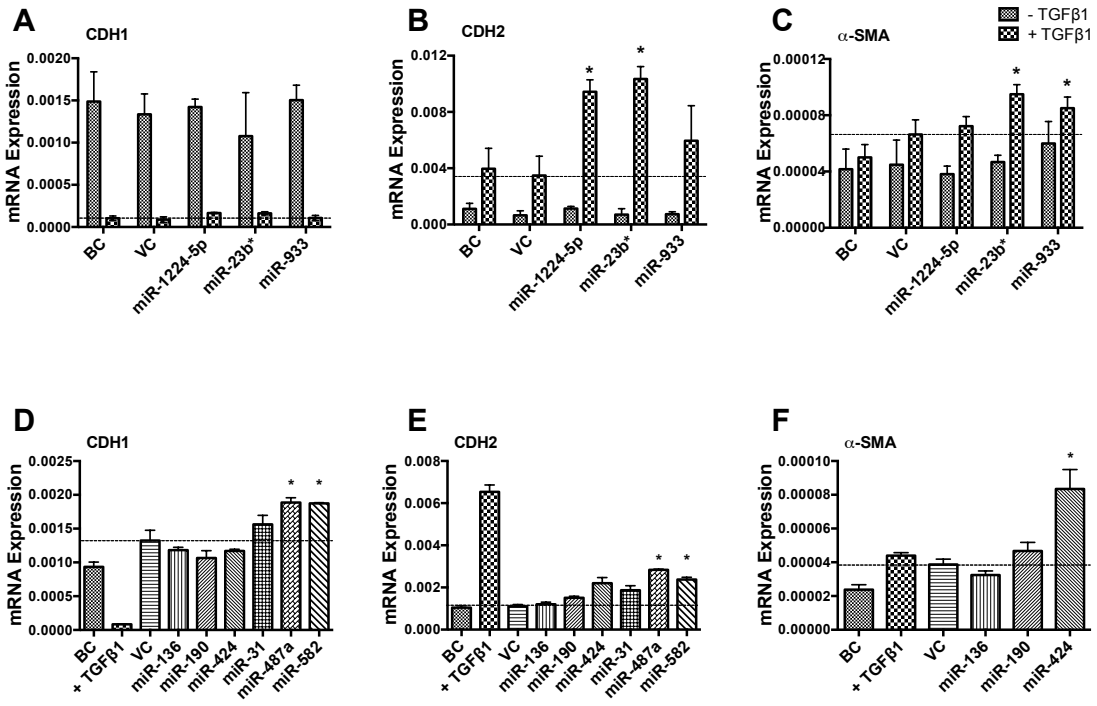

Fig. III. 1.4 Effect of over-expressing miRNAs on the expression of epithelial cell marker and mesenchymal cell markers. A549 cells were infected with a miRNA lenti-virus at a MOI of 50 for 2 days and then treated with TGF-β1 (5 ng/ml) (A-C) or nothing (D-F) for 3 days. mRNA levels of CDH1, CDH2 and α-SMA were measured by real-time PCR and normalized to 18S rRNA. Results are means ± s.e. (two cell preparations, measured in duplicate), except miR-424 which had 5 cell preparations. *$p<0.05$ v.s. VC. BC: Blank control, VC: Virus control.

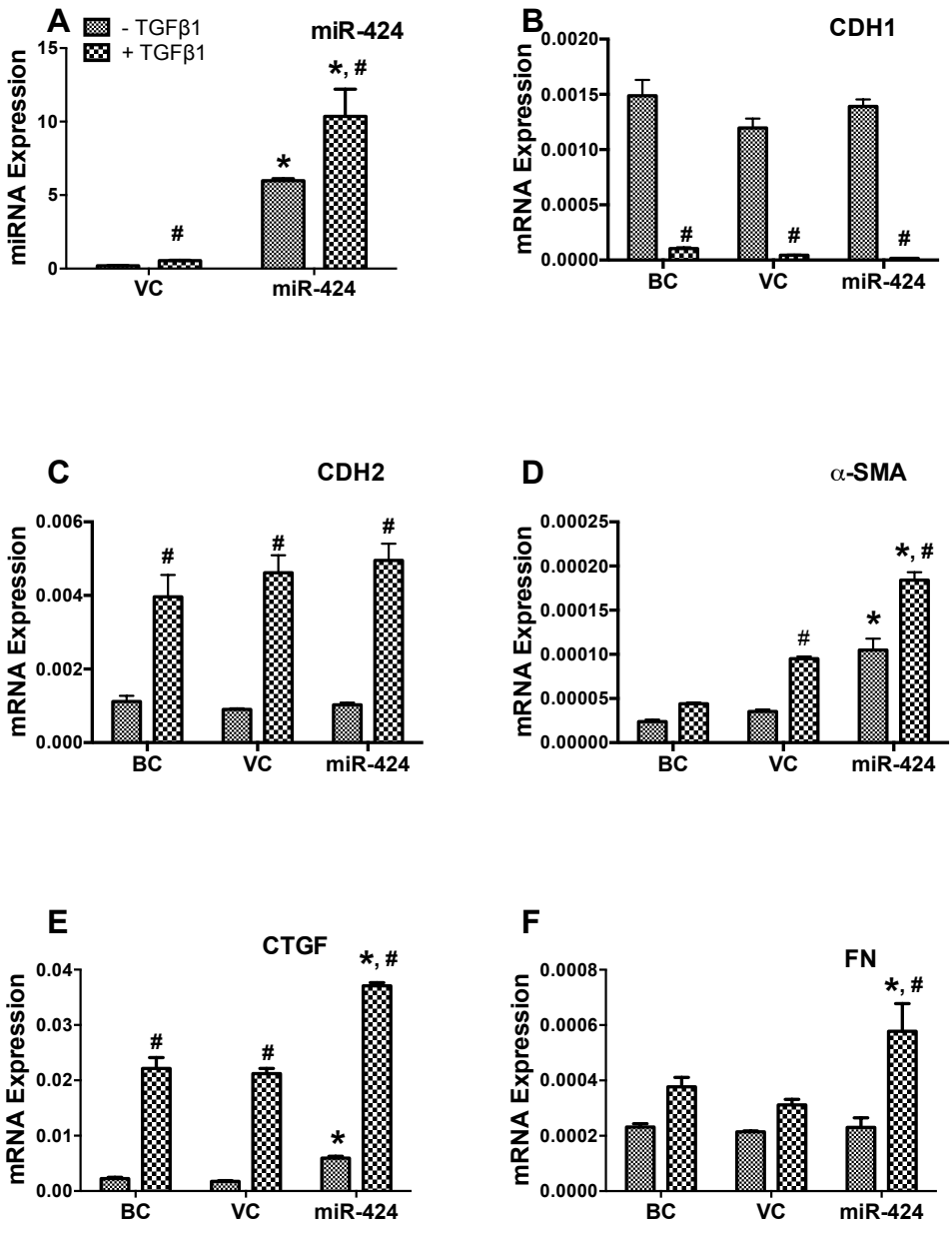

Fig. III. 1.5 Over-expression of miR-424 promotes myofibroblast differentiation during EMT. A549 cells were infected with miR-424 lentivirus at a MOI of 50 for 24 h, followed by TGF-β1 treatment (5 ng/ml) for 72 h. miR-424 and mRNA expressions were determined using real-time PCR. (A) miR-424, (B) CDH1, (C) CDH2, (D) α-SMA, (E) CTGF, and (F) FN. miR-424 expression was normalized to RNU6B, while mRNA expression was normalized to 18S rRNA. BC: Blank control, VC: Virus control, CTGF: Connective tissue growth factor, FN: Fibronectin. Results are means ± s.e. (n=3). *P<0.01 v.s. VC. #P<0.05 v.s. non-TGFβ1 treated control. Two-way ANOVA with Bonferroni post-test.

We further examined the effects of miR-424 on the myofibroblast differentiation during TGF-β1-induced EMT. The miR-424 level was increased by 25 fold when A549 cells were treated with a miR-424 lentivirus (Fig. III. 1.5A). TGF-β1 further increased the miR-424 level in the miR-424 lentivirus-treated cells. While TGF-β1 decreased CDH1 and increased CDH2 mRNA expression, miR-424 had no effect on CDH1 or CDH2 mRNA expression in either the presence or the absence of TGF-β1 (Fig. III. 1.5B, C). However, over-expression of miR-424 increased α-SMA mRNA expression. The combination of miR-424 over-expression with TGF-β1 treatment further increased α-SMA expression compared to TGF-β1 or miR-424 over-expression alone (Fig. III. 1.5D). The same effects were observed for connective tissue growth factor (CTGF), another myofibroblast marker (Fig. III. 1.5E). Although miR-424 overexpression alone had no effect on the fibronectin (FN) mRNA level, the combination of TGF-β1 and miR-424 over-expression increased FN expression (Fig. III. 1.5F). The results suggested that miR-424 may enhance myofibroblast differentiation, but not EMT.

3.1.4 miR-424 enhances activity of the TGF-β signaling pathway

Since miRNAs form many positive and negative regulatory loops, and miR-424 is regulated by TGF-β signaling, we examined whether miR-424 affects the activity of the TGF-β pathway using a TGF-β reporter luciferase assay. TGF-β1 increased the reporter activity in the vector control group. miR-424 alone enhanced the reporter activity to almost the same level as that in the TGF-β1-treated vector control group (Fig. III. 1.6). The combination of miR-424 over-expression and TGF-β1 stimulation further increased the reporter activity. This result indicates that miR-424 potentiates the TGF-β signaling pathway.

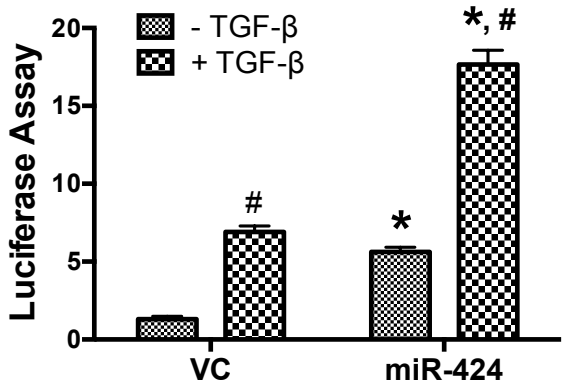

Fig. III. 1.6 miR-424 increases TGF-β signaling activity. HEK 293T cells were co-transfected with 50 ng of the TGF-β signaling reporter plasmid and 100 ng of miR-424 expression plasmid by using Lipofectamine. After 24 h of incubation, the cells were treated with TGF-β1 (5 ng/ml) for 24 h and assayed for dual-luciferase activities. The results shown are mean ± s.e. (n=3). *P<0.001 v.s. vector control (VC). #P<0.001 v.s. non-TGF-β1 treated control.

3.1.5 Smurf2 is a target of miR-424

Since miRNAs negatively regulate their target genes, we would expect that miR-424 targets negative regulators in the TGF-β signaling pathway to enhance TGF-β signaling activity. Using Web-based target predication software (TargetScan, miRand and DIANA-microT), we identified three negative regulators of the TGF-β/Smad signaling (Smad7, Smurf1 and Smurf2) as potential targets of miR-424 (Table III.1). To verify the prediction, we first used a 3'-UTR reporter assay in HEK293 cells. As shown in Fig. III. 1.7A, miR-424 inhibited the 3'-UTR reporter activities of Smad7, Smurf1 and Smurf2. Since miRNA-mediated effects may be cell content-dependent, we further studied whether miR-424 could reduce the endogenous expression of these proteins in A549 cells. We increased the miR-424 expression level in A549 cells using a miR-424 lentivirus at a MOI of 50. Western blotting revealed that the Smurf2, but not Smurf1 or Smad7 protein levels, was significantly decreased in the miR-424-over-expressed cells in comparison with virus control or blank control groups (Fig. III. 1.7B, C). The mRNA expression

levels of the three predicted targets were not affected by miR-424 (Fig. III. 1.7D), suggesting that miR-424 directly inhibits protein translation of Smurf2.

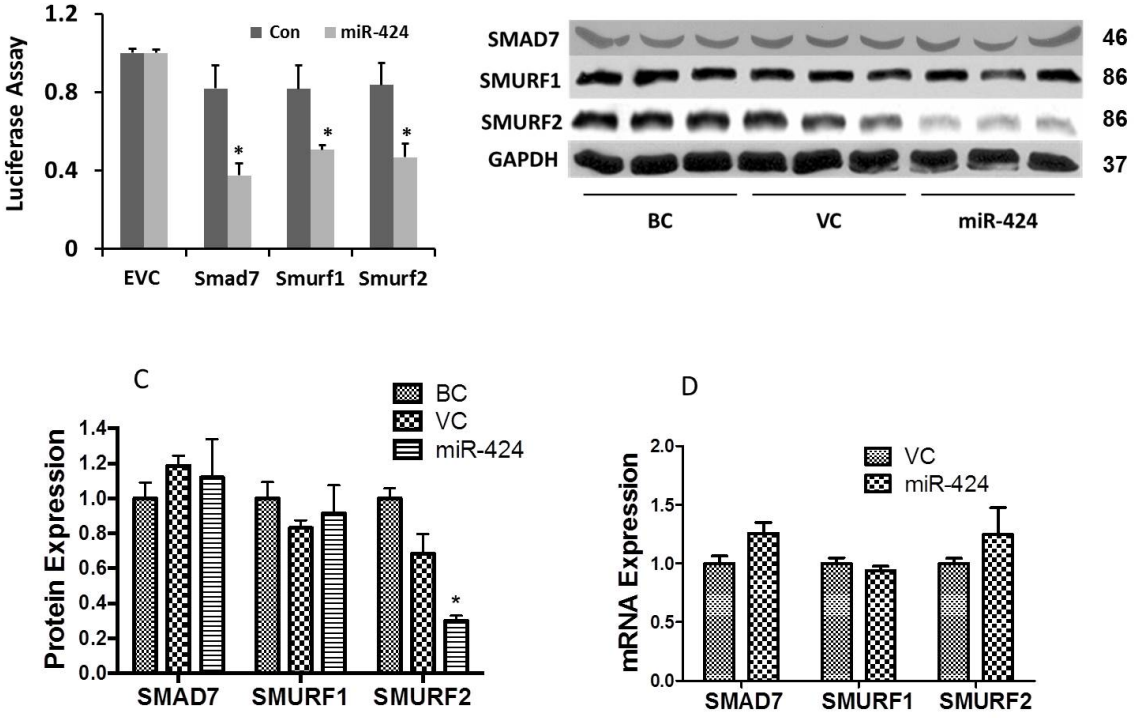

Fig. III. 1.7 Effects of miR-424 on the expression of Smurf2. (A) 3'-UTR reporter assay. 3'-UTR reporter plasmids of Smad7, Smurf1 or Smurf2 were co-transfected with a miR-424 expression vector, or its control vector (Con), into HEK293 cells. The dual luciferase activities were measured and expressed a ratio of firefly to *Renilla* luciferase activity. The results were normalized to the empty vector control without 3'-UTR (EVC) from the two independent experiments, each with 3 replications. *P<0.005 v.s. control. (B-D) A549 cells were infected with a miR-424 lentivirus at a MOI of 50 for 48 h. Protein and mRNA levels of Smad7, Smurf1 and Smurf2 were determined using Western blotting and real-time PCR. (B) Western blot showed the protein expressions of Smurf1, Smurf2 and Smad7. GAPDH was used as a loading control. (C) The quantitation of protein levels from Western blotting using Image J. Data was normalized to GAPDH. (D) mRNA levels of Smurf1, Smurf2 and Smad7 were determined by real-time PCR and normalized to 18S rRNA. BC: Blank control, VC: Virus control. The results shown are means ± s.e. (n=3). *P<0.05 v.s. VC. Two-way ANOVA with bonferroni post-test.

Table III.1: Predicated binding sites of miR-424

	Smad7	Smurf1	Smurf2
miRRanda	42-62	2904-2925	210-232
TargetScan 6.2	55-62	2918-2925 (conserved) 451-457 (poorly conserved)	225-231
DIANA microT 3.0	33-61	2896-2924 931-959 1368-1396	N/A

3.2 EZH2 enhances myofibroblast differentiation in idiopathic pulmonary fibrosis

3.2.1 EZH2 is up-regulated in the lungs of patients with IPF and mice with bleomycin-induced lung fibrosis.

To determine the potential roles of EZH2 in IPF, we first measured the EZH2 mRNA expression in the lung tissues of patients with IPF. The tissues were divided into three groups by the disease severity according to patients' pulmonary function, which was determined by the predicted forced vital capacity (FVC): mild group, > 80%; medium group, 50% - 80% ; and severe group, < 50%. We found that the mRNA expression of EZH2 increased in a fashion of a positive correlation with the severity of the disease (Fig. III.2.1). Both 50% - 80% and < 50% groups had a statistically significant increase in EZH2 mRNA expression compared to > 80% group. EZH2 mRNA expression was the lowest in patients with a FVC of > 80% and was the highest in patient with a FVC of < 50%.

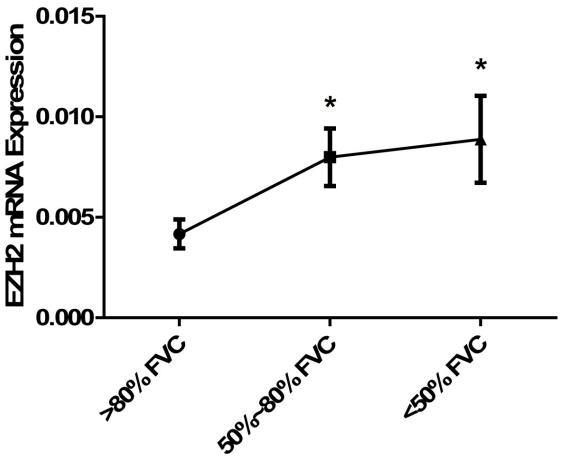

Figure III.2.1: EZH2 expression in the lungs of patients with IPF. Lung tissues from patients with IPF were grouped according to their forced vital capacity (FVC): mild, > 80% (8 patients), medium, 50% - 80% (10 patients), and severe, < 50% (10 patients). The mRNA expression of EZH2 was determined by real-time PCR and normalized to β-actin. The results shown are means ± SE. *P < 0.05 vs. > 80% FVC group (Student T-test).

We also examined the EZH2 expression in the lung tissues of a bleomycin-induced murine lung fibrosis model. Immunohistochemical analysis using EZH2 antibodies showed a strong staining in the bleomycin group whereas signals could be barely detected in the control group (Fig. III.2.2A), suggesting that EZH2 protein is also up-regulated in bleomycin-induced lung fibrosis.

To determine whether the increase in EZH2 protein occurs in myofibroblasts, we performed double-labeling with antibodies against EZH2 and α-SMA, a cellular marker for myofibroblasts. We used ABC staining to detect EZH2 protein and immunofluorescence staining to detect α-SMA protein on the same slide. Positive signals for EZH2 (brown) and α-SMA (green) were observed in the fibrotic foci of lungs from bleomycin-challenged mice. When the images from both staining were overlaid, EZH2 and α-SMA signals were found to be co-localized in the same cells (Fig. III.2.2B). To further confirm this finding, we isolated primary fibroblasts/myofibroblasts from the lungs of mice challenged with bleomycin or PBS (control).

Western blot analysis revealed that EZH2 protein was increased in the fibroblasts/myofibroblasts from bleomycin-challenged mice comparing to these from control mice (Fig. III.2.2C).

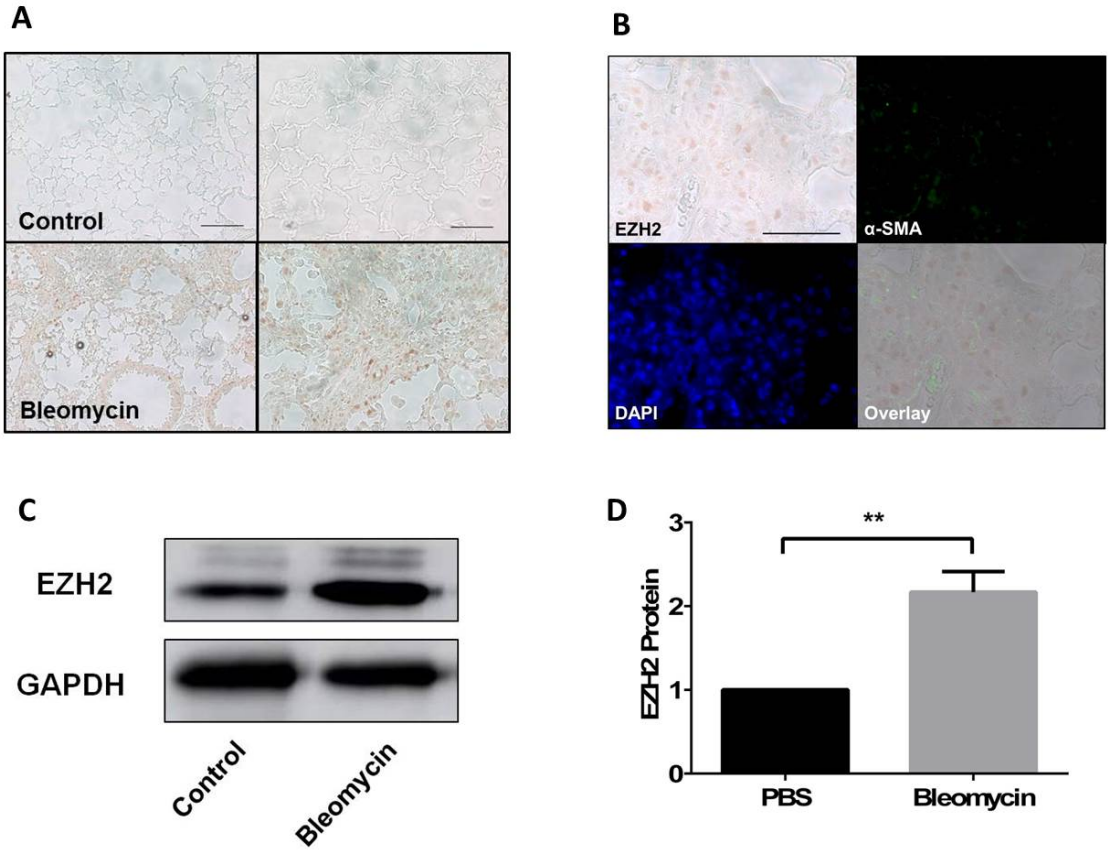

Figure III.2.2: EZH2 expression in the lungs of bleomycin-challenged mice. (A) Lung tissue sections of PBS-(control) and bleomycin-challenged mice were stained with anti-EZH2 antibodies and ABC staining. EZH2 was shown as brown color. Scale bars: left, 100 µm and right, 50 µm. (B) Lung tissue sections were double-labeled with ABC staining using anti-EZH2 antibodies and immunofluorescence staining using anti-α-SMA antibodies. Nuclei were stained with DAPI. Overlay of EZH2 and α-SMA stainings showed co-localization of two proteins. Scale bar: 50 µm. (C) Primary fibroblasts/myofibroblasts were isolated from PBS control and bleomycin-challenged mice. EZH2 protein levels were determined by western blotting. Quantitation of western blot results was performed using Image J software and normalized to GADPH. The results shown are means ± SE from 3 independent experiments, in which each experiment used different generations of primary fibroblasts/myofibroblasts from 4 animals (2 control and 2 bleomycin-challenged mice). *P < 0.05 (Student T-test).

3.2.2 EZH2 is required for the TGFβ1-induced differentiation of fibroblasts to myofibroblasts.

To determine the function of EZH2 in IPF, we examined the effect of EZH2 inhibition on the differentiation of fibroblasts to myofibroblasts. We used the EZH2 inhibitor 3-Deazaneplanocin A (DZNep) for this purpose. DZNep inhibits S-adenosylhomocystine (AdoHcy) hydrolase, which leads to the accumulation of AdoHcy. An increased level of AdoHcy inhibits the EZH2 protein level in cells [117-121]. Human lung fibroblasts (LL29) were treated with DZNep and then stimulated with TGFβ1. Western blot analysis showed that TGFβ1 had no effects on EZH2 protein expression. However, DZNep reduced the EZH2 protein level in both basal and TGFβ1-stimulated cells (Fig. III.2.3A, B). TGFβ1 increased mRNA and protein expression of α-SMA and the reduction of EZH2 level by DZNep inhibited the TGFβ1-induced α-SMA (Fig. III.2.3A, C, D). Furthermore, the mRNA levels of fibronectin (FN) and COLA4A1, the markers of fibroblast activation, was also induced by TGFβ1, but was inhibited by DZNep (Fig. III.2.3 E, F).

Contractility is one of the characteristics of fibroblasts/myofibroblasts and myofibroblasts have a stronger contractility compared to fibroblasts [72]. We measured contractility using a gel contraction assay [122, 123]. LL29 cells were pre-treated DZNep, followed by TGFβ1 stimulation. The cells were trypsinized and mixed with collagen. After polymerization, the gels were detached from the bottom of the wells. Cell contractility causes the shrinkage of the gel (Fig. III.2.4A) and thus the surface area of the gel reflects cell contractility. TGFβ1-treated cells showed a smaller surface area comparing to these without TGFβ1 treatment. The inhibition of EZH2 by DZNep significantly increased the gel surface area in both basal and TGFβ1-stimulated cells (Fig. III.2.4B), indicating that DZNep reduced fibroblasts/myofibroblasts contractility.

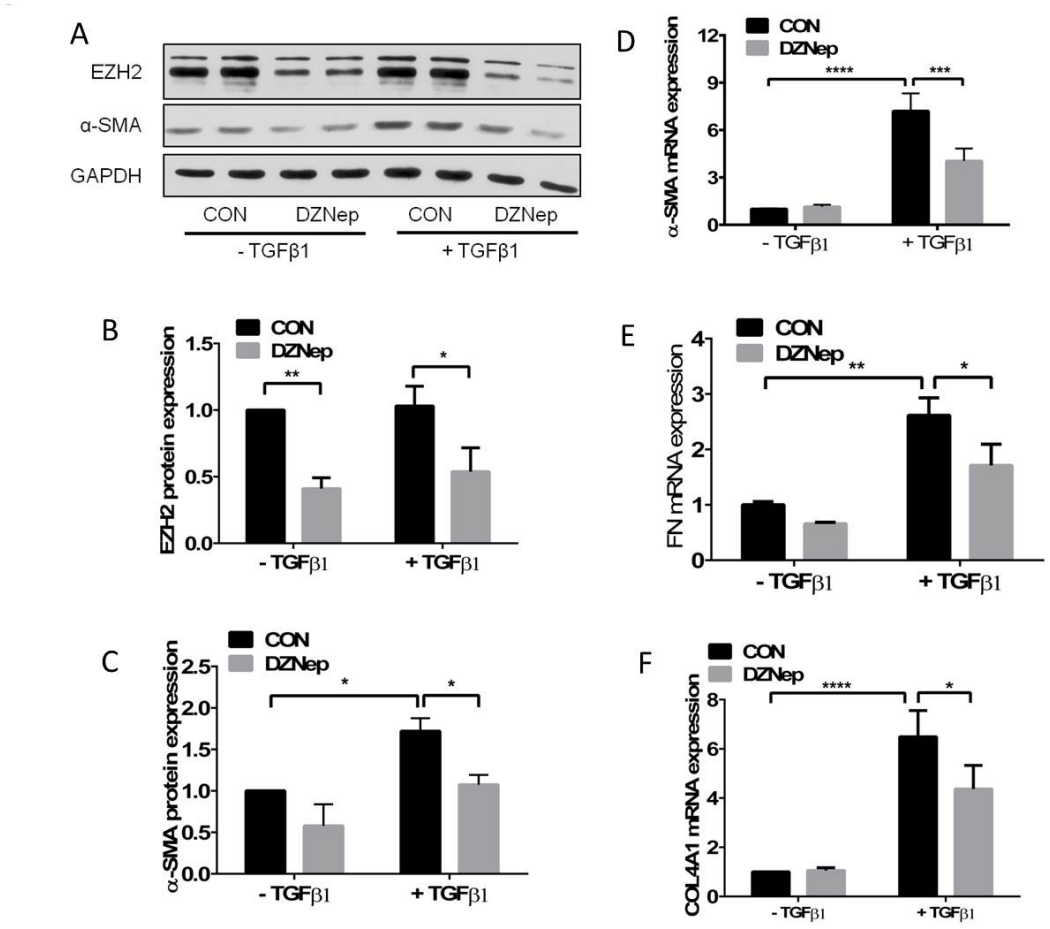

Figure III.2.3: TGFβ1-induced myofibroblast marker expression is inhibited by EZH2 inhibitor DZNep. LL29 cells were treated with DZNep (4 μM) for 24 hours and then with DZNep and TGFβ1 (5 ng/ml) together for additional 24 hours. The cells without DZNep treatment was used as a control (CON). EZH2 and α-SMA protein expression was measured using western blotting. GAPDH was used as a loading control. Representative blots are shown in (A) and quantitation results using ImageJ software were normalized to GAPDH and are shown in (B) and (C). The mRNA levels of α-SMA (D), fibronectin (FN) (E) and COL4A1 (F) were determined using real-time PCR and normalized to β-actin. All the results are means ± SE from three independent experiments, each performed in duplication. *P < 0.05, **P < 0.01, ***P < 0.001, ****P < 0.0001, (ANOVA and Fisher's LSD).

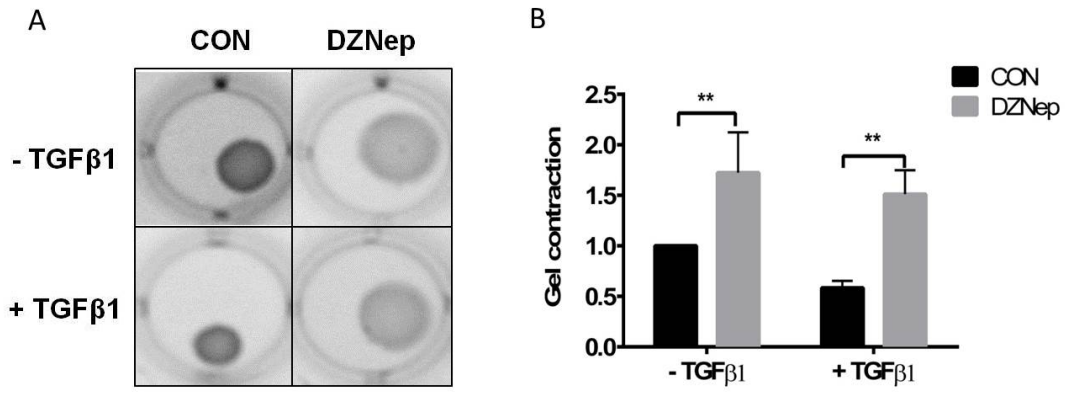

Figure III.2.4: TGFβ1-induced contractility is inhibited by EZH2 inhibitor DZNep. (A) LL29 cells were treated with DZNep (4 μM) for 24 hours and then with DZNep and TGFβ1 (5 ng/ml) together for additional 24 hours. The cells were mixed with Collagen 1 and added to 12-well plates. Gel was detached from well wall and bottom and the images were taken after 48 hours. (A) Representative images. (B) Gel surface area was measured using Image J software. Results shown are means ± SE from three independent experiments (n = 3) with duplication in each experiment. ** $P < 0.01$ (ANOVA and Fisher's LSD).

To further confirm the inhibitor study, we reduced EZH2 protein level using gene silencing. LL29 cells were infected with EZH2 shRNA or control lentivirus at a MOI of 50 and then stimulated the cells with TGFβ1. Western blot analysis showed a reduction in EZH2 and α-SMA protein level in the EZH2 shRNA-treated cells (Fig. III.2.5A, B). Taken all together, our results suggest that the reduction of EZH2 level inhibits the differentiation of fibroblasts to myofibroblasts.

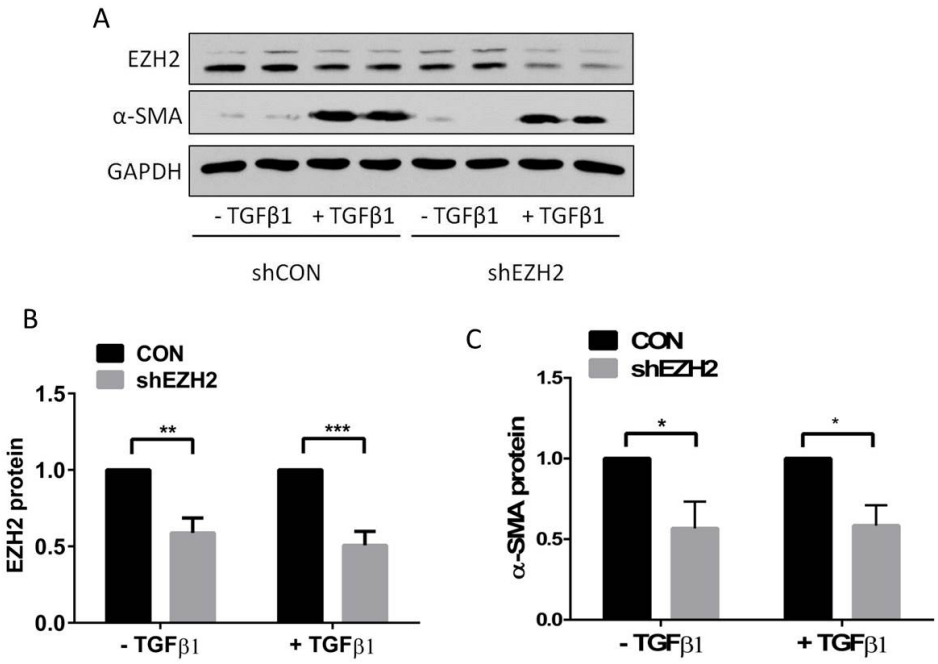

Figure III.2.5: EZH2 knock-down decreases myofibroblast marker α-SMA. LL29 cells were infected with a lentivirus containing shEZH2 or its control shCON at a MOI of 100 for 24 hours. 48 hours after infection, the cells were treated with 5 ng/ml of TGFβ1 for another 24 hours. EZH2 and α-SMA protein levels were determined by western blotting. **(A)** Representative blots. **(B, C)** Quantitation of western blotting results using Image J software. The results were normalized to GAPDH and expressed as a percent of shCON. Data shown are means ± SE from three independent experiments, each performed in duplicate. ***$P < 0.001$ (Student T test).

3.2.3 EZH2 inhibition reduces p-Smad2/3 nuclear translocation via its interaction with Smad2/3.

TGFβ signaling is initiated by the binding of TGFβ to the complex of transmembrane receptor serine/threonine kinases (TβRI and II) on cell membrane. The activated TβRI phosphorylates Smad2/3, which form a complex with Smad4. The Smad complex then translocates into the nucleus and regulates the transcription of down-stream target genes. To explore how EZH2 affects TGFβ signaling, we first determined whether DZNep affects the phosphorylation of Smad2/3. LL29 cells were treated with DZNep for 48 hours and then stimulated with TGFβ1 for 30, 60 and 120 minutes. TGFβ treatment resulted in the

phosphorylation of Smad2/3 as determined by western blotting using antibodies against phosphorylated Smad2/3. However, DZNep had little effect on the phosphorylation of Smad2/3 (Fig. III.2.6).

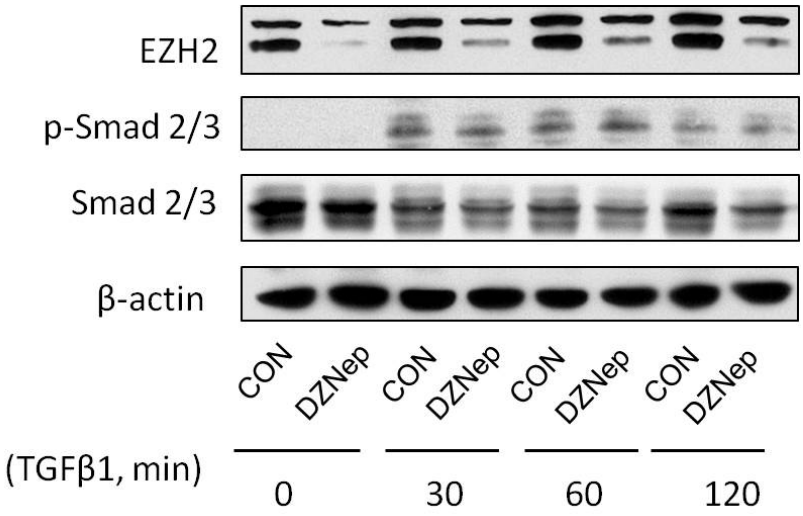

Figure III.2.6: Phosphorylation of Smad2/3 is not affected by DZNep. LL29 cells were treated with 4 μM of DZNep for 48 hours and then with TGFβ1 (5 ng/ml) for 30, 60 or 120 minutes. Western blotting was performed to detect the protein levels of EZH2, p-Smad2/3, Smad 2/3 and β-actin. Representative results are shown from three independent experiments.

We next determined whether DZNep affects p-Smad2/3 nuclear translocation. LL29 cells were treated with DZNep for 48 hours and stimulated with TGFβ1 for 60 minutes. The nucleus was separated from cytosol. Sole localizations of cytoplasmic marker GAPDH in cytosol and nuclear marker lamin B1 in nucleus confirmed the separation of nuclear and cytosol (Fig. III.2.7). EZH2 was only located in the nucleus and its protein level was reduced by DZNep treatment. p-Smad2 and p-Smad3 were only detected in the TGFβ1-treated group, in which DZNep decreased the level of p-Smad2/3 in nucleus, but increased them in cytosol. This result indicates that the inhibition of EZH2 reduces p-Smad2/3 nuclear translocation.

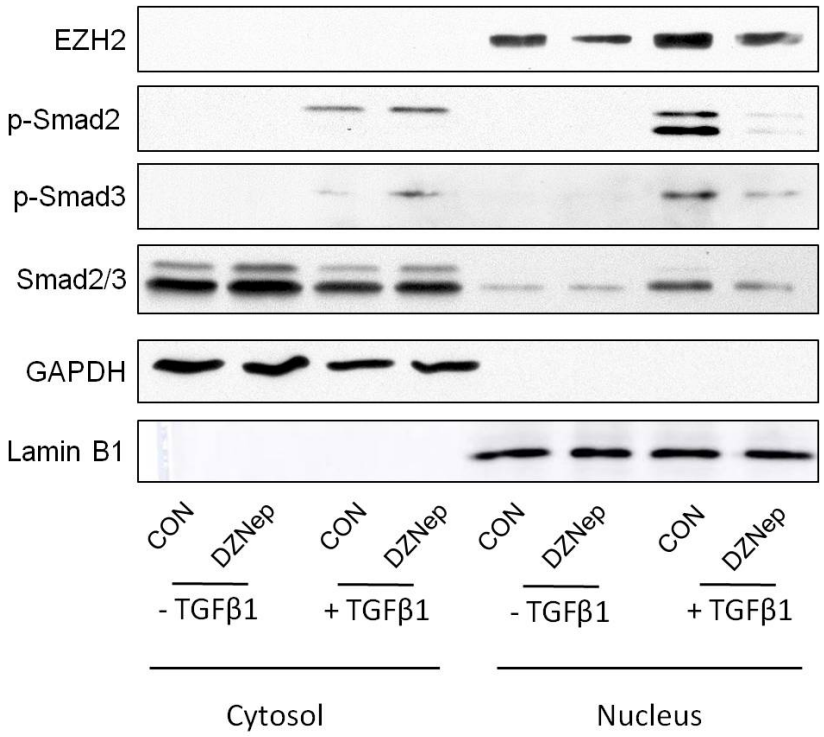

Figure III.2.7: DZNep inhibits phospho-Smad2/3 nuclear translocation. LL29 cells were treated with DZNep (4 μM) or none (CON) for 48 hours and then with TGFβ1 (5 ng/ml) for 60 minutes. Protein levels of EZH2, p-Smad 2, p-Smad3 and Smad 2/3 in cytoplasmic and nuclear fractions were determined by Western blotting. GAPDH and lamin B1 were used as cytosol and nucleus loading controls. Representative results were shown from three independent experiments.

EZH2 has binding motifs which could interact with other protein molecules. We reasoned that EZH2 could directly interact with Smad2/3 in nucleus, resulting in the increased p-Smad2/3 nuclear translocation by retaining them in the nucleus. To test this hypothesis, we performed a Co-immunoprecipitation (Co-IP) experiment to detect a physical interaction between EZH2 and Smad2/3. LL29 cell lysates were immunoprecipitated with anti-EZH2 antibodies and the complex was detected for Smad2/3 by western blotting. Most of the EZH2 was pulled-down with anti-EZH2 antibodies and Smad2/3 were detected in the immunoprecipitates (Fig. III.2.8). Since DZNep reduces EZH2 protein expression, less EZH2 and Smad2/3 was observed in the immunoprecipitates. The result suggests an interaction between EZH2 and Smad2/3.

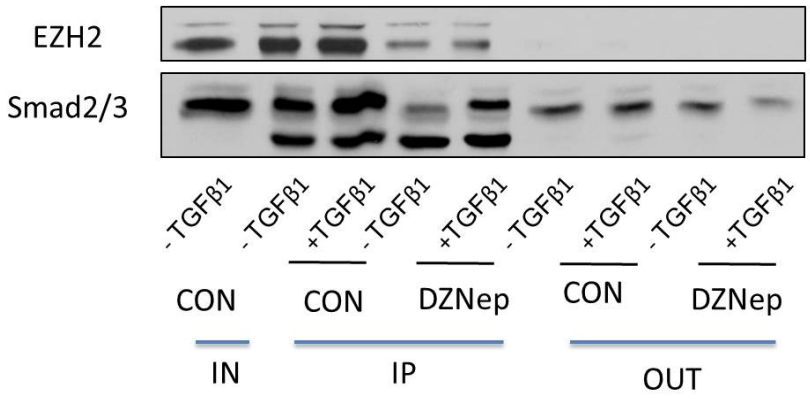

Figure III.2.8: EZH2 directly interacts with Smad2/3. LL29 cells were pre-treated with 4 μM of DZNep for 24 hours and then with 5 ng of TGFβ1 and 4 μM of DZNep for another 24 hours. The cell lysates were immunoprecipitated with anti-EZH2 antibodies. EZH2 and Smad2/3 in the complex were determined by western blotting. Representative results were shown from three independent experiments. IN: total cell lysate; IP: pulled-down protein; OUT: cell lysate after pull-down.

3.2.4 DZNep attenuates the severity of bleomycin-induced lung fibrosis

To determine the in vivo effect of EZH2 inhibition on lung fibrosis, we delivered DZNep to mice daily starting one day before bleomycin challenge through intraperitoneal route. Lung tissues were collected on day 17. Bleomycin increased the mRNA expression of EZH2 by 10-fold compared to PBS group (6.96 ± 1.46×10-6 vs. 6.98 ± 3.54×10-5), and DZNep treatment attenuated the increase by 77% (Fig. III.2.9A). Similar changes were observed for EZH2 protein with a 10.8-fold increase in the bleomycin group compared to control group and a 73% inhibition by DZNep (Fig. III.2.9B). This result confirmed the effectiveness of DZNep treatment in vivo in reducing EZH2 expression levels.

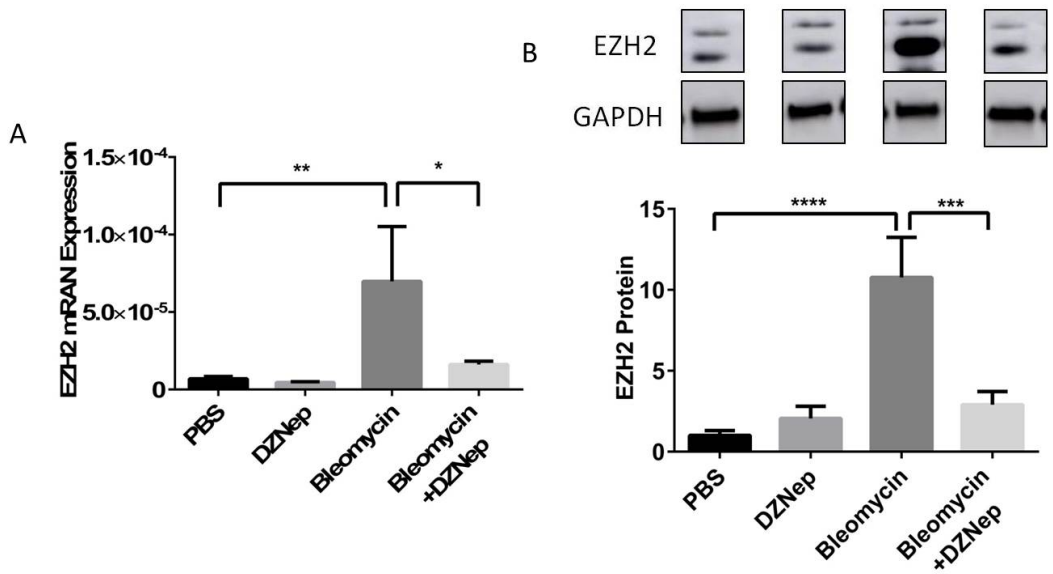

Figure III.2.9: DZNep inhibits bleomycin-induced EZH2 mRNA and protein expression in mice. Female C57BL/6 mice were challenged with PBS or bleomycin intratracheally and treated with PBS or DZNep through intraperitoneal injection once per day starting on one day before bleomcyin challenge. Left lung tissue was collected on day 17. **(A)** mRNA level of EZH2 was determined using real-time PCR and normalized to 18S rRNA. EZH2 protein level was determined by western blotting. Representative blots and quantitation were shown in **(B).** The results were normalized to GAPDH. Data shown are means ± SE. n = 6 animals in each group *$P < 0.05$, **$P < 0.01$, *** $P < 0.001$, **** $P < 0.0001$ (ANOVA and Fisher's LSD).

H & E staining showed that while the lung tissue of mice was normal in both PBS and DZNep group, there were thickened alveolar septa and fibroblasts/myofibroblasts foci found in the lung tissue of bleomycin-treated mice. The lungs of the bleomycin plus DZNep group exhibited a marked reduction in fibrotic areas (Fig. III.2.10A). The severity of fibrosis then was evaluated using a semi-quantitative histological scoring system introduced by Ashcroft [115]. Generally, a higher Ashcroft score represents more severe fibrosis histologically. Ashcroft scores in PBS and DZNep groups were zero. In the bleomycin-challenged group, the Ashcroft score was 5.09 ± 0.27, which was reduced to 3.43 ± 0.64 by DZNep treatment (Fig. III.2.10B).

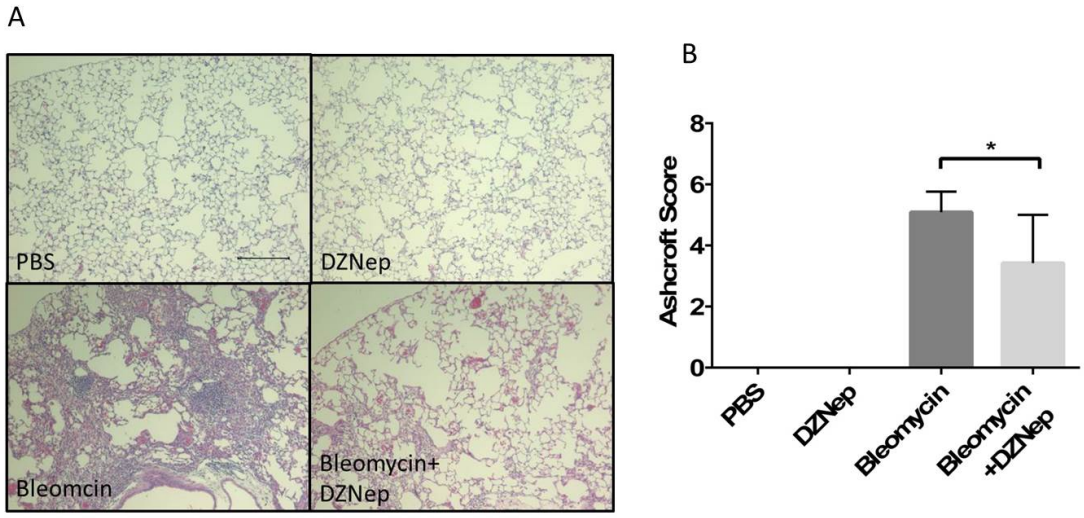

Figure III.2.10: DZNep attenuates pulmonary fibrosis histologically. Female C57BL/6 mice were challenged with PBS or bleomycin intratracheally and treated with PBS or DZNep through intraperitoneal injection once per day starting on one day before bleomcyin challenge. Right lung tissue was collected on day 17 and stained with hematoxylin and eosin. **(A)** Representative images. Scale bar: 200 μm. **(B)** Ashcroft scale system was used to quantify pulmonary fibrosis. All the results are means ± SE. n = 6 animals in each group. *$P < 0.05$ (Student T-test).

To further assess the severity of lung fibrosis in each group, we measured mRNA and/or protein expression of myofibroblast markers. The mRNA level of α-SMA, as expected, was up-regulated by 73% using bleomycin challenge (7.61 ± 1.62 ×10-5 vs. 13.2 ± 0.2 ×10-5) and this increase was decreased 37% by DZNep treatment (Fig. III.2.11A). Similar changes were observed for the mRNA expression of COL1A1 and COL3A1 (Fig. III.2.11B, C). α-SMA protein was also up-regulated in the bleomycin-treated group and down-regulated by DZNep treatment (Fig. III.2.11D). All the results suggest that DZNep reduces the severity of bleomycin-induced fibrosis in the lungs.

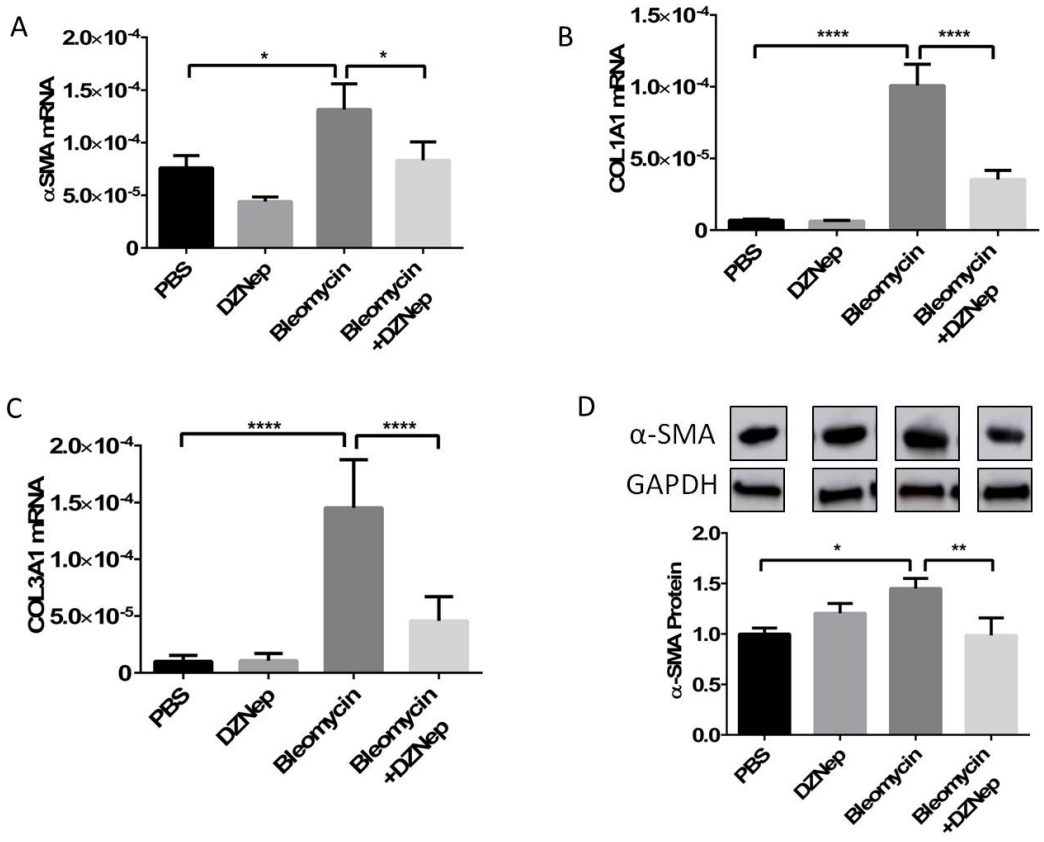

Figure III.2.11: DZNep inhibits fibrotic markers in mice lungs. Female C57BL/6 mice were challenged with PBS or bleomycin intratracheally and treated with PBS or DZNep through intraperitoneal injection once per day starting on one day before bleomcyin challenge. Left lung tissue was collected on day 17. The mRNA levels of fibrotic markers α-SMA **(A)**, COL1A1 **(B),** and COL3A1 **(C)** were determined using real-time PCR and normalized to 18S rRNA. α-SMA protein level was determined using western blotting. Representative blots and quantitation were shown in **(B)**. The results were normalized to GAPDH. All the results are means ± SE. n = 6 animals in each group. **P* < 0.05, ***P* < 0.01, **** *P* < 0.0001 (ANOVA and Fisher's LSD).

CHAPTER IV

DISCUSSION

4.1 miR-424 and EMT

The purpose of this study was to identify specific miRNAs that have roles in EMT during IPF. First, we identified 6 up-regulated and 3 down-regulated miRNAs in the TGF-β-induced EMT model of human lung epithelial cells through miRNA microarray analysis. One of these up-regulated miRNAs, miR-424, enhanced the expression of α-SMA without affecting epithelial or mesenchymal cell markers. miR-424 also increased the activity of the TGF-β signaling pathway and decreased the protein expression of Smurf2, a negative regulator of TGF-β signaling. Our results suggest that miR-424 regulates the myofibroblast differentiation during EMT by potentiating the TGF-β signaling pathway, likely through Smurf2.

miRNAs have been reported to regulate EMT in a variety of cell lines. Previous studies have shown that the miR-200 family and miR-205 are gradually down-regulated during TGF-β1-mediated EMT. The manipulation of their levels affects EMT in renal epithelial cells by targeting ZEB1 and SIP1 [87]. The miR-200 family is also down-regulated in IPF patients, and regulates EMT in rat alveolar epithelial cells (AECs) [124]. A number of other miRNAs have also been reported to be involved in lung fibrotic diseases, including miR-21, miR-155, miR-29 and let-7d [86, 88, 90-92]. However, direct miRNA microarray analysis of EMT in lung epithelial cells has not been reported yet. In this study, we identified 9 miRNAs which were changed during EMT of

the lung epithelial cells. Among these 9 miRNAs, only miR-31 has been shown to have a role in EMT by inhibiting the activation of lung fibroblasts through directly targeting integrin α(5) and RhoA [124].

The changes in miRNAs during EMT do not necessarily mean that the altered miRNAs have functional roles in EMT. Indeed, using the gain-of-function approach, we found that only miR-424 markedly increased α-SMA expression. α-SMA is considered to be a marker for myofibroblasts and an indicator for myofibroblast differentiation [90, 125, 126]. In lung fibrotic diseases, the persistence of myofibroblasts is an important indicator of the end stage of the disease [72, 127, 128]. Myofibroblasts have stronger contractile activity and are more responsive to inflammatory factors than fibroblasts [129]. Thus, the increase in myofibroblasts in the diseased lung may reduce lung compliance, enhance extracellular matrix production, disrupt the basement membrane and cause inflammation and epithelial injury [44, 130]. It is still not clear what causes myofibroblast differentiation. Several factors have been studied including mechanical stretch, specialized matrix proteins, inflammatory factors, and the TGF-β signaling pathway [72, 131, 132].

A number of studies have characterized regulators of α-SMA transcription. Smad3, a key transcription factor in the Smad-dependent TGF-β signaling pathway, induces α-SMA expression through its binding with two CAGA motifs, called Smad3-binding elements (SBEs), in the promoter of the α-SMA gene [133]. Smad3-independent signaling via p38 and MEK/ERK also contributes to α-SMA regulation [134]. Sp1/Sp3 binding to the MCAT enhancer is also considered to be necessary for α-SMA expression [135]. In addition to the TGF-β signaling pathway, other mechanisms have also been reported to regulate the expression of α-SMA [72]. The Notch/CSL pathway regulates α-SMA expression through its promoter activity [136]. CCAAT/enhancer binding protein β (C/EBPβ) also induces α-SMA expression in lung fibroblasts

[137]. The transcription repressor, Gut-enriched Krüppel-like factor, negatively regulates α-SMA by preventing the binding of Smad3 to SBEs [138].

miR-424 has not previously been reported to be involved in any of the pathways mentioned above. Our studies found that miR-424 enhanced the activity of Smad-dependent TGF-β signaling, as revealed by a TGF-β signaling reporter assay. This result suggests that the up-regulation of α-SMA produced by miR-424 likely occurs through potentiating TGF-β signaling. The reporter plasmid we used has a transcription response element (TRE) which can be activated by the Smad2/3/4 complexes, and thus the activity of the reporter represents the activity of the Smad-dependent TGF-β signaling pathway. The Smads are well-studied intracellular effectors of the TGF-β signaling pathway. There are three groups of Smads: receptor-activated Smads (R-Smads, Smad2/3), a common Smad (Smad4), and inhibitory Smads (Smad7). Upon ligand binding, R-Smads are phosphorylated by phosphorylated type II receptors. The phosphorylation of R-Smads on their C-terminal SXS motif results in changes of their conformation, causing the exposure of interacting interfaces and two R-Smads, either homomeric or heteromeric, and one common Smad form a trimeric complex, which then dissociates from the receptors and is translocated into the nucleus, where it acts as a transcription factor regulating numerous transcriptional activities [139]. The inhibitory Smad, Smad7, inhibits the TGF-β signaling pathway by competitively interfering with R-Smad recruitment and phosphorylation by TGF-β receptors [139, 140]. The TGF-β signaling pathway forms an inhibitory feedback loop through the induction of Smad7 expression [141].

Smurf2, another known TGF-β signaling negative regulator, belongs to the family of Smad ubiquitin regulatory factors (Smurfs), which are HECT-domain-containing E3 ligases. They are748 amino acids long and have several distinctive structural features as compared to other E3 ligases, including a phospholipid/calcium-binding C2 domain and WW domains [142]. Smurf2 has been reported to directly interact with Smad2 and Smad3 through the linker region

containing a PY motif, which is recognized by the WW domain, causing proteasome-dependent degradation of Smad2 and Smad3 [143-145]. In addition, Smurf2 can also form a complex with Smad7, which then is exported from the nucleus to the cytoplasm and targets the activated TGF-β type I receptor to proteasomes for degradation through ubiquitination [145, 146].

By using web-based target prediction databases, we found that three inhibitory regulators of the TGF-β signaling pathway, Smad7, Smurf1 and Smurf2, were potential targets of miR-424. Western blotting showed that the protein level of Smurf2, but not Smurf1 or Smad7, was significantly decreased after over-expression of miR-424. Furthermore, the mRNA level of Smurf2 was unchanged by miR-424, indicating that the protein change of Smurf2 was not due to mRNA cleavage but because of translation, which is the major mechanism of miRNAs in animals. Although Smurf1 and Smurf2 share most of the same sequence, Smurf2 acts as a specific negative regulator for the Smad signaling pathway [142]. This explains why miR-424 can enhance TGF-β signaling by only decreasing the protein level of Smurf2, but not Smurf1.

miR-424 promoted myofibroblast differentiation, but did not promote EMT in response to TGF-β treatment, even though the TGF-β signaling pathway regulates both processes. The mechanisms remain to be identified. We speculate that the disparate effects of miR-424 on these two processes are due to the specificity of Smad2 and Smad3 in downstream gene expression. Knockout of Smad2, but not Smad3, prevents EMT [147], indicating that Smad2 is involved in EMT. On the other hand, as mentioned above, Smad3 is believed to be the main regulator of TGF-β mediated α-SMA expression [72, 133, 138]. Although Smurf2 has been shown to cause the degradation of TβRI, the Smad2 and Smad3 in vitro [143-146] and in vivo study of Smurf2 knockout mice reveals that Smurf2 does not cause the degradation of Smad2, Smad3 or the TGF-β type I receptor. However, it does induce the multiple mono-ubiquitination of the Smad3 MH2 domain to inhibit the formation of Smad3 complexes [142]. This suggests that Smurf2 acts by

specifically inhibiting Smad3. Thus, the reduction of Smurf2 by miR-424 enhances the activity of Smad3, leading to enhanced α-SMA expression after EMT.

In summary, we demonstrated a two-step process of EMT: first, human lung epithelial cells lose epithelial characteristics and gain mesenchymal markers to become fibroblast-like cells, which can be induced by TGF-β treatment alone; and second, the fibroblast-like cells differentiate into myofibroblasts, in which miR-424 potentiates TGF-β signaling (Fig. IV.1).

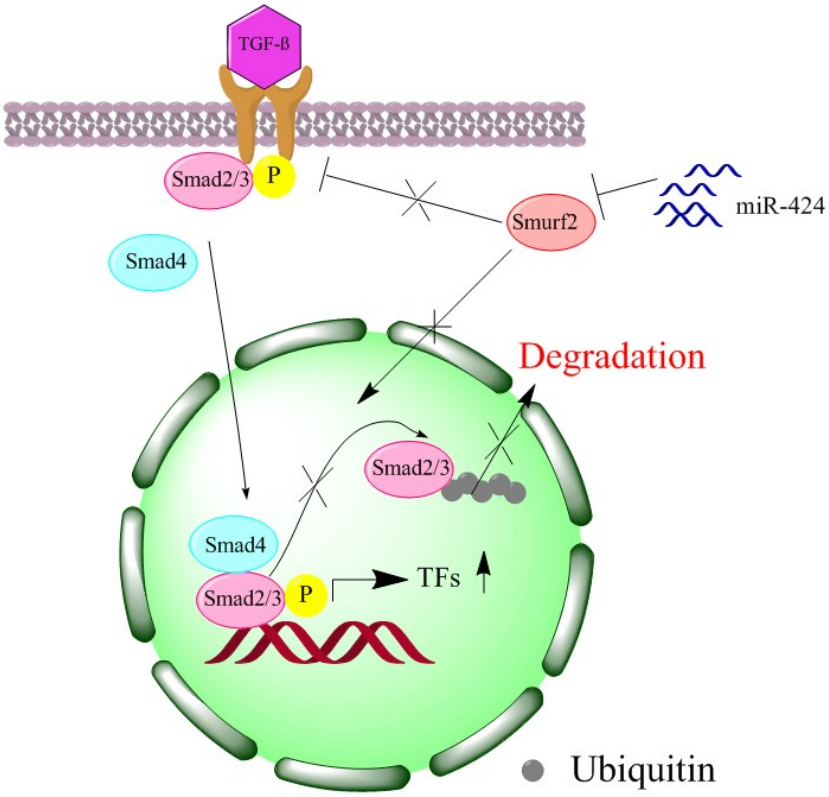

Figure IV.1: miR-424 targets Smurf2 to potentiates TGF-β signaling pathway. Inhibiton of Smurf2 by miR-424 decreases ubiquitination and degradation of Smad2/3, which further induces transcriptional factors.

4.2 EZH2 and fibroblast differentiation

Previous studies on EZH2 have mainly been focused on its histone methyltransferase activity [96, 100-102, 148-150]. The purpose of this study was to examine the role of EZH2 in the development of IPF. We found that EZH2 was up-regulated in the lungs of patients with IPF and bleomycin-challenged mice. The inhibition of EZH2 by inhibitor DZNep or EZH2 shRNA reduced fibroblast activation in vitro and in vivo. This effect is mediated by EZH2 enhancement of TGF-β signaling pathway likely through direct binding of EZH2 with Smad2/3 and thus retaining Smad2/3 in the nucleus.

IPF and cancer share some common characteristics [105, 106, 151]. Several signaling pathways such as the Wnt/β-catenin signaling pathway are abnormally activated in both IPF and cancer [152] [153]. The global DNA methylation patterns observed in patients with IPF have partial similarity to these in cancer [42, 43]. Approximately 10% of the miRNAs are significantly changed in IPF and some of them are involved in this disease [76, 86, 88, 90, 92, 104]. Many miRNAs also contribute the pathogenesis of cancer [154, 155]. By taking advantage of the knowledge from cancer, we may better understand the pathogenesis of IPF [105].

Down-regulation of miR-101 in cancer leads to the over-expression of its target EZH2, which further results in cancer progression [103, 104]. The over-expression of EZH2 is associated with prostate cancer, breast cancer, bladder cancer and lung cancer [100, 101]. Although EZH2 has extensively been studied in several human cancers, its role in IPF is still unknown. Similar to cancer, we found that EZH2 was up-regulated in IPF and its expression level was inversely correlated to pulmonary functions in patients with IPF. EZH2 was co-localized with myofibroblast marker α-SMA in bleomycin-challenged mice. This result was confirmed by the observation that EZH2 expression was higher in primary fibroblasts/myofibroblasts isolated from bleomycin-challenged mice that these from control mice. Up-regulation of EZH2 in α-SMA-

expressing myofibroblasts suggests that EZH2 may be involved in the regulation of differentiation of fibroblasts to myofibroblasts.

Uncontrolled extracellular matrix production in IPF is originated from fibroblastic foci [45, 46, 127]. Resident fibroblasts, epithelial cells (via EMT), and fibrocytes contribute to the formation of the foci [6]. Three factors are known to induce the differentiation of fibroblasts to myofibroblasts: local accumulation of active TGFβ1, high extracellular mechanical stress, and the presence of specialized ECM protein [72]. The current study also showed that TGFβ1 treatment of human fibroblasts increased the expression of α-SMA and ECM proteins such as Fn and COL4A1 as well as collagen gel contractility. EZH2 inhibitor DZNep reduced TGFβ-induced expression of these proteins and gel contractility. These data suggest that the inhibition of EZH2 with DZNep prevent the differentiation of fibroblasts to myofibroblasts.

DZNep is the cyclopentanyl analog of 3-deazaadanosin and inhibits S-adenosylhomocysteine (AdoHcy) hydrolase. AdoHcy hydrolase is responsible for the hydrolysis of S-adenosylhomocysteine to adenosine and homocysteine. The inhibition of AdoHcy hydrolase causes the accumulation of AdoHcy, which in turn results in the inhibition of S-adonosyl-L-methionine-dependent methyltransferase [117-121]. DZNep has been reported to decrease the protein level of EZH2, and has been used as a specific inhibitor of EZH2 [148-150, 156-159]. Since DZNep serves as an indirect inhibitor of EZH2, we used gene silencing to confirm the inhibitor studies. Similar to the inhibitor studies, the reduction of EZH2 level by EZH2 shRNA also reduced α-SMA protein level in TGFβ1-treated fibroblasts.

TGF-β signaling pathway is involved in α-SMA expression and myofibroblast differentiation [160, 161]. Smad3, upon phosphorylation, binds with the Smad3-binding elements (SBEs) in the α-SMA promoter to induce α-SMA expression in myofibroblasts [133]. Smad3 is also required for ECM secretion in myofibroblasts [162].

TGF-β signaling pathway is regulated by many mechanisms [77]. The increase in the phosphorylation of Smad2/3 activates TGF-β signaling. However, the inhibition of EZH2 using DZNep had no effect on total Smad2/3 or phosphorylated Smad2/3. Thus this is not likely the mechanism of EZH2-mediated myofibroblast differentiation.

The dynamic distribution of Smads between the cytoplasm and nucleus poses a tight regulation of the TGFβ signaling pathway. The translocation of phosphorylated Smads from the cytoplasm into the nucleus is considered as a rate-limiting step in the TGF-β signal transduction. The exporting of Smads out of the nucleus to the cytoplasm turns off the signaling. Nuclear import factors moleskin (Msk), importin 7 (Imp7), and Imp8 are responsible for Smad nuclear import [163, 164] by interacting with nucleoporins including Sec13, Nup75, Nup93, and Nup205 [165]. For Smad nuclear export, exportin 4 and RanBP3 have been reported to be involved [166, 167]. Our result indicates that the inhibition of EZH2 reduced Smad2/3 accumulation in the nucleus and in turns reduced the activity of the TGF-β signaling pathway.

Several mechanisms regulate Smad trafficking between the cytoplasm and nucleus [168]. Mono-ubiquitination of Smad4 by the ubiquitin ligase TIF1γ reduced the accumulation of Smad4 [169]. Phosphorylation in the linker region by cyclin-dependent kinases (CDKs) and MAPK inhibits Smad translocation [170, 171]. A kinetic analysis of Smad nucleocytoplasmic trafficking shows that nuclear mobility of Smad2 and Smad4 and nuclear export rate of Smad2 are decreased in TGFβ1-treated cells, indicating active Smads are trapped in the nucleus [172]. The Smad trapping can be explained as a result of retaining of Smads via their interaction with other proteins in the nucleus. The transcription factor Yes-associated protein (YAP) and transcriptional co-activator with PDZ-binding motif (TAZ) have been shown to directly bind Smads to retain Smads in the nucleus [173, 174].

EZH2 can interact with several proteins. EZH2 bind EED, SUZ12, and other proteins to form PRC2, which catalyzed H3K27me3 and it interacts with transcription factor YY1 [97, 98]. A recent study demonstrated that EZH2 was able to bind Smad2 and Smad4 directly [175]. Our Co-IP study in pulmonary fibroblasts showed that EZH2 interacts with Smad2 and Smad3. Thus, we propose that EZH2 enhances TGFβ signaling pathway by retaining active Smad2/3 in nucleus via interaction between EZH2 and Smad2/3. As a result, EZH2 increases α-SMA expression and induces myofibroblast differentiation.

Several animal models of experimental lung fibrosis have been developed for studying the pathogenesis of IPF, including exposure to bleomycin, silica, fluorescein isothiocyanate, irradiation, or expression of specific genes using a transgenic system [176]. Bleomycin is an anti-cancer chemotherapeutic drug that causes pulmonary fibrosis as a major adverse drug effect. It breaks DNA strand directly as well as induces oxidative stress to cause fibrosis [177]. Although bleomycin model has some limitations [176, 177], a single dose of intratracheal delivery of bleomycin remains the mostly frequently used method, mainly due to its easily delivery, short time in inducing fibrosis, and some histological hallmarks similar to IPF.

Using intratracheally delivery of a single dose of bleomycin model [178], we found that EZH2 was significantly up-regulated. This model provides us a tool to evaluate the effect of EZH2 inhibitor DZNep on pulmonary fibrosis in vivo. DZNep does not have any obvious toxicity when administrated at a dose of 10 mg/kg single dose [179]. The effects of DZNep in various cancer models have been reported. Intravenous administration of DZNep inhibits angiogenesis in a subcutaneous glioblastoma mouse model without toxicities [180]. Intraperitoneal delivery of DZNep and histone deacetylase inhibitor panobinostat increases animal survival in an acute myeloid leukemia mouse model [150]. In the leukemia-engrafted mouse model of AML, intraperitoneal administration of DZNep reduces tumor growth and prolongs the survival of animals [181]. DZNep-treated prostate cancer cells showed reduced tumorigenicity in vivo [182].

In this study, we found that intraperitoneal administration of DZNep reduced pulmonary fibrosis in bleomycin-induced pulmonary fibrosis mouse model.

In summary, we discovered that EZH2 is up-regulation of EZH2 in IPF and it promotes the differentiation of pulmonary fibroblasts to myofibroblasts. We also revealed a new mechanism of EZH2 action, i.e. enhancing TGFβ signaling pathway retaining Smad2/3 in the nucleus via a direct interaction between EZH2 and Smad2/3 (Fig. IV.2). In vivo studies showed inhibition of EZH2 by DZNep reduced pulmonary fibrosis.

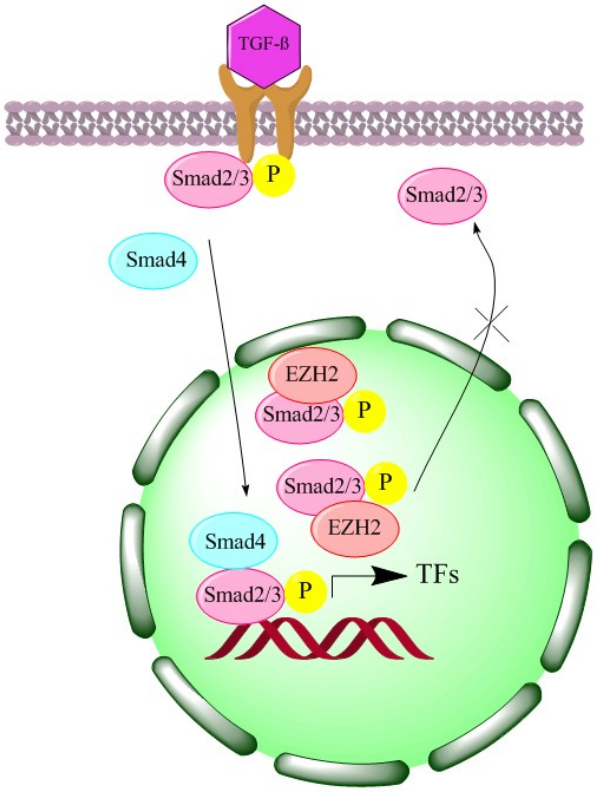

Figure IV.2: EZH2 retains phosphor-Smad2/3 in the nucleus. Up-regulated EZH2 binds to phosphor-Smad2/3 to induce the accumulation of phosphor-Smad2/3.

CHAPTER V

SUMMARY AND CONCLUSION

Idiopathic pulmonary fibrosis (IPF) is one of the most common and severe interstitial lung diseases. The etiology is still unknown. Understanding the pathogenesis of IPF will provide therapeutic targets for treating this disease.

EMT has been shown to participate in the process of IPF. A number of miRNAs have been reported to be involved in fibrotic diseases. However, no direct evidence has been presented to show that miRNAs regulate EMT in human lung epithelial cells. We identified 6 up-regulated and 3 down-regulated miRNAs in a human lung epithelial cell EMT model using miRNA microarray and real-time PCR. Overexpression of one of these up-regulated miRNAs, miR-424, increased the expression of α-smooth muscle actin, an indicator of myofibroblast differentiation, but had no effects on the epithelial or mesenchymal cell markers. miR-424 enhanced the activity of the TGF-β signaling pathway, as demonstrated by a luciferase reporter assay. Further experiments showed that miR-424 decreased the protein expression of Smurf2, a negative regulator of TGF-β signaling, indicating that miR-424 exerts a forward regulatory loop in the TGF-β signaling pathway. Our results suggest that miR-424 regulates the myofibroblast differentiation during EMT by potentiating the TGF-β signaling pathway, likely through Smurf2.

Fibroblastic foci represent a hallmark of the histopathology of IPF. They are composed of fibroblasts/myofibroblasts. Abnormally activated/differentiated myofibroblasts exaggerate the ECM accumulation. We investigated the role of EZH2 in the differentiation of fibroblasts into myofibroblasts and underlying mechanisms. We found that EZH2 was up-regulated in the lungs of patients with IPF and mice with bleomycin-induced lung fibrosis. The up-regulation of EZH2 occurred in myofibroblasts. The inhibition of EZH2 by its inhibitor DZNep or shRNA reduced TGFβ1-induced differentiation of human lung fibroblasts into myofibroblasts as demonstrated by the expression of myofibroblast marker α-smooth muscle actin, fibronectin and COLA4A1 as well as contractility. DZNep inhibited Smad2/3 nuclear translocation without affecting Smad2/3 phosphorylation. Co-immunoprecipitation revealed a direct interaction between EZH2 and Smad2/3. DZNep treatment attenuated bleomycin-induced pulmonary fibrosis in mice. We conclude that EZH2 induces the differentiation of fibroblasts to myofibroblasts by binding and retaining Smad2/3 in the nucleus.

In summary, we demonstrated a two-step process of EMT: first, human lung epithelial cells lose epithelial characteristics and gain mesenchymal markers to become fibroblast-like cells, which can be induced by TGF-β treatment alone; and second, the fibroblast-like cells differentiate into myofibroblasts, in which miR-424 potentiates TGF-β signaling. We also discovered that EZH2 is up-regulation of EZH2 in IPF and it promotes the differentiation of pulmonary fibroblasts to myofibroblasts. We also revealed a new mechanism of EZH2 action, i.e. enhancing TGFβ signaling pathway retaining Smad2/3 in the nucleus via a direct interaction between EZH2 and Smad2/3. In vivo studies showed inhibition of EZH2 by DZNep reduced pulmonary fibrosis. Our study on the roles of miR-424 in EMT and of EZH2 in fibroblast differentiation could lead to further development of antifibrotic drugs.

REFERENCES

1. Raghu, G., et al., An official ATS/ERS/JRS/ALAT statement: idiopathic pulmonary fibrosis: evidence-based guidelines for diagnosis and management. Am J Respir Crit Care Med, 2011. 183(6): p. 788-824.

2. Visscher, D.W. and J.L. Myers, Histologic spectrum of idiopathic interstitial pneumonias. Proc Am Thorac Soc, 2006. 3(4): p. 322-9.

3. Coultas, D.B., et al., The epidemiology of interstitial lung diseases. Am J Respir Crit Care Med, 1994. 150(4): p. 967-72.

4. Nalysnyk, L., et al., Incidence and prevalence of idiopathic pulmonary fibrosis: review of the literature. Eur Respir Rev, 2012. 21(126): p. 355-61.

5. Ley, B., H.R. Collard, and T.E. King, Jr., Clinical course and prediction of survival in idiopathic pulmonary fibrosis. Am J Respir Crit Care Med, 2011. 183(4): p. 431-40.

6. King, T.E., Jr., A. Pardo, and M. Selman, Idiopathic pulmonary fibrosis. Lancet, 2011. 378(9807): p. 1949-61.

7. Baumgartner, K.B., et al., Cigarette smoking: a risk factor for idiopathic pulmonary fibrosis. Am J Respir Crit Care Med, 1997. 155(1): p. 242-8.

8. Faner, R., et al., Abnormal lung aging in chronic obstructive pulmonary disease and idiopathic pulmonary fibrosis. Am J Respir Crit Care Med, 2012. 186(4): p. 306-13.

9. Hubbard, R., et al., Occupational exposure to metal or wood dust and aetiology of cryptogenic fibrosing alveolitis. Lancet, 1996. 347(8997): p. 284-9.

10. Miyake, Y., et al., Occupational and environmental factors and idiopathic pulmonary fibrosis in Japan. Ann Occup Hyg, 2005. 49(3): p. 259-65.

11. Egan, J.J., et al., Epstein-Barr virus replication within pulmonary epithelial cells in cryptogenic fibrosing alveolitis. Thorax, 1995. 50(12): p. 1234-9.

12. Ueda, T., et al., Idiopathic pulmonary fibrosis and high prevalence of serum antibodies to hepatitis C virus. Am Rev Respir Dis, 1992. 146(1): p. 266-8.

13. Irving, W.L., S. Day, and I.D. Johnston, Idiopathic pulmonary fibrosis and hepatitis C virus infection. Am Rev Respir Dis, 1993. 148(6 Pt 1): p. 1683-4.

14. Raghu, G., et al., High prevalence of abnormal acid gastro-oesophageal reflux in idiopathic pulmonary fibrosis. Eur Respir J, 2006. 27(1): p. 136-42.

15. Gribbin, J., R. Hubbard, and C. Smith, Role of diabetes mellitus and gastro-oesophageal reflux in the aetiology of idiopathic pulmonary fibrosis. Respir Med, 2009. 103(6): p. 927-31.

16. Idiopathic Pulmonary Fibrosis Clinical Research, N., et al., Randomized trial of acetylcysteine in idiopathic pulmonary fibrosis. N Engl J Med, 2014. 370(22): p. 2093-101.

17. Idiopathic Pulmonary Fibrosis Clinical Research, N., et al., Prednisone, azathioprine, and N-acetylcysteine for pulmonary fibrosis. N Engl J Med, 2012. 366(21): p. 1968-77.

18. Elmufdi, F., et al., Novel mechanisms and treatment of idiopathic pulmonary fibrosis. Discov Med, 2015. 20(109): p. 145-53.

19. Nogee, L.M., et al., A mutation in the surfactant protein C gene associated with familial interstitial lung disease. N Engl J Med, 2001. 344(8): p. 573-9.

20. Thomas, A.Q., et al., Heterozygosity for a surfactant protein C gene mutation associated with usual interstitial pneumonitis and cellular nonspecific interstitial pneumonitis in one kindred. Am J Respir Crit Care Med, 2002. 165(9): p. 1322-8.

21. Chibbar, R., et al., Nonspecific interstitial pneumonia and usual interstitial pneumonia with mutation in surfactant protein C in familial pulmonary fibrosis. Mod Pathol, 2004. 17(8): p. 973-80.

22. van Moorsel, C.H., et al., Surfactant protein C mutations are the basis of a significant portion of adult familial pulmonary fibrosis in a dutch cohort. Am J Respir Crit Care Med, 2010. 182(11): p. 1419-25.

23. Lawson, W.E., J.E. Loyd, and A.L. Degryse, Genetics in pulmonary fibrosis--familial cases provide clues to the pathogenesis of idiopathic pulmonary fibrosis. Am J Med Sci, 2011. 341(6): p. 439-43.

24. Lawson, W.E., et al., Endoplasmic reticulum stress in alveolar epithelial cells is prominent in IPF: association with altered surfactant protein processing and herpesvirus infection. Am J Physiol Lung Cell Mol Physiol, 2008. 294(6): p. L1119-26.

25. Steele, M.P. and D.A. Schwartz, Molecular mechanisms in progressive idiopathic pulmonary fibrosis. Annu Rev Med, 2013. 64: p. 265-76.

26. Korfei, M., et al., Epithelial endoplasmic reticulum stress and apoptosis in sporadic idiopathic pulmonary fibrosis. Am J Respir Crit Care Med, 2008. 178(8): p. 838-46.

27. Wang, Y., et al., Genetic defects in surfactant protein A2 are associated with pulmonary fibrosis and lung cancer. Am J Hum Genet, 2009. 84(1): p. 52-9.

28. Maitra, M., et al., Surfactant protein A2 mutations associated with pulmonary fibrosis lead to protein instability and endoplasmic reticulum stress. J Biol Chem, 2010. 285(29): p. 22103-13.

29. Batista, L.F., et al., Telomere shortening and loss of self-renewal in dyskeratosis congenita induced pluripotent stem cells. Nature, 2011. 474(7351): p. 399-402.

30. Armanios, M.Y., et al., Telomerase mutations in families with idiopathic pulmonary fibrosis. N Engl J Med, 2007. 356(13): p. 1317-26.

31. Tsakiri, K.D., et al., Adult-onset pulmonary fibrosis caused by mutations in telomerase. Proc Natl Acad Sci U S A, 2007. 104(18): p. 7552-7.

32. Alder, J.K., et al., Short telomeres are a risk factor for idiopathic pulmonary fibrosis. Proc Natl Acad Sci U S A, 2008. 105(35): p. 13051-6.

33. Cronkhite, J.T., et al., Telomere shortening in familial and sporadic pulmonary fibrosis. Am J Respir Crit Care Med, 2008. 178(7): p. 729-37.

34. Seibold, M.A., et al., A common MUC5B promoter polymorphism and pulmonary fibrosis. N Engl J Med, 2011. 364(16): p. 1503-12.

35. Peljto, A.L., et al., The pulmonary fibrosis-associated MUC5B promoter polymorphism does not influence the development of interstitial pneumonia in systemic sclerosis. Chest, 2012. 142(6): p. 1584-8.

36. Coward, W.R., et al., Defective histone acetylation is responsible for the diminished expression of cyclooxygenase 2 in idiopathic pulmonary fibrosis. Mol Cell Biol, 2009. 29(15): p. 4325-39.

37. Coward, W.R., et al., Repression of IP-10 by interactions between histone deacetylation and hypermethylation in idiopathic pulmonary fibrosis. Mol Cell Biol, 2010. 30(12): p. 2874-86.

38. Sanders, Y.Y., et al., Thy-1 promoter hypermethylation: a novel epigenetic pathogenic mechanism in pulmonary fibrosis. Am J Respir Cell Mol Biol, 2008. 39(5): p. 610-8.

39. Cisneros, J., et al., Hypermethylation-mediated silencing of p14(ARF) in fibroblasts from idiopathic pulmonary fibrosis. Am J Physiol Lung Cell Mol Physiol, 2012. 303(4): p. L295-303.

40. Huang, S.K., et al., Histone modifications are responsible for decreased Fas expression and apoptosis resistance in fibrotic lung fibroblasts. Cell Death Dis, 2013. 4: p. e621.

41. Hu, B., et al., Essential role of MeCP2 in the regulation of myofibroblast differentiation during pulmonary fibrosis. Am J Pathol, 2011. 178(4): p. 1500-8.

42. Rabinovich, E.I., et al., Global methylation patterns in idiopathic pulmonary fibrosis. PLoS One, 2012. 7(4): p. e33770.

43. Sanders, Y.Y., et al., Altered DNA methylation profile in idiopathic pulmonary fibrosis. Am J Respir Crit Care Med, 2012. 186(6): p. 525-35.

44. Selman, M., et al., Idiopathic pulmonary fibrosis: prevailing and evolving hypotheses about its pathogenesis and implications for therapy. Ann Intern Med, 2001. 134(2): p. 136-51.

45. Enomoto, N., et al., Quantitative analysis of fibroblastic foci in usual interstitial pneumonia. Chest, 2006. 130(1): p. 22-9.

46. Flaherty, K.R., et al., Fibroblastic foci in usual interstitial pneumonia: idiopathic versus collagen vascular disease. Am J Respir Crit Care Med, 2003. 167(10): p. 1410-5.

47. Thiery, J.P., et al., Epithelial-mesenchymal transitions in development and disease. Cell, 2009. 139(5): p. 871-90.

48. Kang, Y. and J. Massague, Epithelial-mesenchymal transitions: twist in development and metastasis. Cell, 2004. 118(3): p. 277-9.

49. Nakajima, Y., et al., Mechanisms involved in valvuloseptal endocardial cushion formation in early cardiogenesis: roles of transforming growth factor (TGF)-beta and bone morphogenetic protein (BMP). Anat Rec, 2000. 258(2): p. 119-27.

50. Arnoux, V., et al., Erk5 controls Slug expression and keratinocyte activation during wound healing. Mol Biol Cell, 2008. 19(11): p. 4738-49.

51. Ahmed, N., et al., Molecular pathways regulating EGF-induced epithelio-mesenchymal transition in human ovarian surface epithelium. Am J Physiol Cell Physiol, 2006. 290(6): p. C1532-42.

52. Hanahan, D. and R.A. Weinberg, Hallmarks of cancer: the next generation. Cell, 2011. 144(5): p. 646-74.

53. Thiery, J.P., Epithelial-mesenchymal transitions in tumour progression. Nat Rev Cancer, 2002. 2(6): p. 442-54.

54. Perl, A.K., et al., A causal role for E-cadherin in the transition from adenoma to carcinoma. Nature, 1998. 392(6672): p. 190-3.

55. Yang, J., et al., Twist, a master regulator of morphogenesis, plays an essential role in tumor metastasis. Cell, 2004. 117(7): p. 927-39.

56. Chapman, H.A., Epithelial-mesenchymal interactions in pulmonary fibrosis. Annu Rev Physiol, 2011. 73: p. 413-35.

57. Kalluri, R. and E.G. Neilson, Epithelial-mesenchymal transition and its implications for fibrosis. J Clin Invest, 2003. 112(12): p. 1776-84.

58. Iwano, M., et al., Evidence that fibroblasts derive from epithelium during tissue fibrosis. J Clin Invest, 2002. 110(3): p. 341-50.

59. Zeisberg, E.M., et al., Endothelial-to-mesenchymal transition contributes to cardiac fibrosis. Nat Med, 2007. 13(8): p. 952-61.

60. Marmai, C., et al., Alveolar epithelial cells express mesenchymal proteins in patients with idiopathic pulmonary fibrosis. Am J Physiol Lung Cell Mol Physiol, 2011. 301(1): p. L71-8.

61. Yao, H.W., et al., TGF-beta1 induces alveolar epithelial to mesenchymal transition in vitro. Life Sci, 2004. 76(1): p. 29-37.

62. Willis, B.C., et al., Induction of epithelial-mesenchymal transition in alveolar epithelial cells by transforming growth factor-beta1: potential role in idiopathic pulmonary fibrosis. Am J Pathol, 2005. 166(5): p. 1321-32.

63. Kim, K.K., et al., Alveolar epithelial cell mesenchymal transition develops in vivo during pulmonary fibrosis and is regulated by the extracellular matrix. Proc Natl Acad Sci U S A, 2006. 103(35): p. 13180-5.

64. Fontana, L., et al., Fibronectin is required for integrin alphavbeta6-mediated activation of latent TGF-beta complexes containing LTBP-1. FASEB J, 2005. 19(13): p. 1798-808.

65. Munger, J.S., et al., The integrin alpha v beta 6 binds and activates latent TGF beta 1: a mechanism for regulating pulmonary inflammation and fibrosis. Cell, 1999. 96(3): p. 319-28.

66. Xu, M.Y., et al., Lysophosphatidic acid induces alphavbeta6 integrin-mediated TGF-beta activation via the LPA2 receptor and the small G protein G alpha(q). Am J Pathol, 2009. 174(4): p. 1264-79.

67. Jenkins, R.G., et al., Ligation of protease-activated receptor 1 enhances alpha(v)beta6 integrin-dependent TGF-beta activation and promotes acute lung injury. J Clin Invest, 2006. 116(6): p. 1606-14.

68. Kim, Y., et al., Integrin alpha3beta1-dependent beta-catenin phosphorylation links epithelial Smad signaling to cell contacts. J Cell Biol, 2009. 184(2): p. 309-22.

69. Selman, M. and A. Pardo, Role of epithelial cells in idiopathic pulmonary fibrosis: from innocent targets to serial killers. Proc Am Thorac Soc, 2006. 3(4): p. 364-72.

70. Andersson-Sjoland, A., et al., Fibrocytes are a potential source of lung fibroblasts in idiopathic pulmonary fibrosis. Int J Biochem Cell Biol, 2008. 40(10): p. 2129-40.

71. Larsson, O., et al., Fibrotic myofibroblasts manifest genome-wide derangements of translational control. PLoS One, 2008. 3(9): p. e3220.

72. Hinz, B., et al., The myofibroblast: one function, multiple origins. Am J Pathol, 2007. 170(6): p. 1807-16.

73. Wang, R., et al., Human lung myofibroblast-derived inducers of alveolar epithelial apoptosis identified as angiotensin peptides. Am J Physiol, 1999. 277(6 Pt 1): p. L1158-64.

74. Waghray, M., et al., Hydrogen peroxide is a diffusible paracrine signal for the induction of epithelial cell death by activated myofibroblasts. FASEB J, 2005. 19(7): p. 854-6.

75. Kulasekaran, P., et al., Endothelin-1 and transforming growth factor-beta1 independently induce fibroblast resistance to apoptosis via AKT activation. Am J Respir Cell Mol Biol, 2009. 41(4): p. 484-93.

76. Xiao, X., et al., Regulation of myofibroblast differentiation by miR-424 during epithelial-to-mesenchymal transition. Arch Biochem Biophys, 2015. 566: p. 49-57.

77. Derynck, R. and Y.E. Zhang, Smad-dependent and Smad-independent pathways in TGF-beta family signalling. Nature, 2003. 425(6958): p. 577-84.

78. Warner, D.R., R.M. Greene, and M.M. Pisano, Cross-talk between the TGFbeta and Wnt signaling pathways in murine embryonic maxillary mesenchymal cells. FEBS Lett, 2005. 579(17): p. 3539-46.

79. Thiery, J.P. and J.P. Sleeman, Complex networks orchestrate epithelial-mesenchymal transitions. Nat Rev Mol Cell Biol, 2006. 7(2): p. 131-42.

80. Willis, B.C. and Z. Borok, TGF-beta-induced EMT: mechanisms and implications for fibrotic lung disease. Am J Physiol Lung Cell Mol Physiol, 2007. 293(3): p. L525-34.

81. Katoh, Y. and M. Katoh, Hedgehog signaling, epithelial-to-mesenchymal transition and miRNA (review). Int J Mol Med, 2008. 22(3): p. 271-5.

82. Sun, W., et al., microRNA: a master regulator of cellular processes for bioengineering systems. Annu Rev Biomed Eng, 2010. 12: p. 1-27.

83. Berezikov, E., E. Cuppen, and R.H. Plasterk, Approaches to microRNA discovery. Nat Genet, 2006. 38 Suppl: p. S2-7.

84. Majoros, W.H. and U. Ohler, Spatial preferences of microRNA targets in 3' untranslated regions. BMC Genomics, 2007. 8: p. 152.

85. Erson, A.E. and E.M. Petty, MicroRNAs in development and disease. Clin Genet, 2008. 74(4): p. 296-306.

86. Pandit, K.V., J. Milosevic, and N. Kaminski, MicroRNAs in idiopathic pulmonary fibrosis. Transl Res, 2011. 157(4): p. 191-9.

87. Gregory, P.A., et al., The miR-200 family and miR-205 regulate epithelial to mesenchymal transition by targeting ZEB1 and SIP1. Nat Cell Biol, 2008. 10(5): p. 593-601.

88. Pandit, K.V., et al., Inhibition and role of let-7d in idiopathic pulmonary fibrosis. Am J Respir Crit Care Med, 2010. 182(2): p. 220-9.

89. Banyard, J., et al., Identification of genes regulating migration and invasion using a new model of metastatic prostate cancer. BMC Cancer, 2014. 14: p. 387.

90. Liu, G., et al., miR-21 mediates fibrogenic activation of pulmonary fibroblasts and lung fibrosis. J Exp Med, 2010. 207(8): p. 1589-97.

91. Pottier, N., et al., Identification of keratinocyte growth factor as a target of microRNA-155 in lung fibroblasts: implication in epithelial-mesenchymal interactions. PLoS One, 2009. 4(8): p. e6718.

92. Cushing, L., et al., miR-29 is a major regulator of genes associated with pulmonary fibrosis. Am J Respir Cell Mol Biol, 2011. 45(2): p. 287-94.

93. Rea, S., et al., Regulation of chromatin structure by site-specific histone H3 methyltransferases. Nature, 2000. 406(6796): p. 593-9.

94. Cao, R. and Y. Zhang, SUZ12 is required for both the histone methyltransferase activity and the silencing function of the EED-EZH2 complex. Mol Cell, 2004. 15(1): p. 57-67.

95. Pasini, D., et al., Suz12 is essential for mouse development and for EZH2 histone methyltransferase activity. EMBO J, 2004. 23(20): p. 4061-71.

96. Chase, A. and N.C. Cross, Aberrations of EZH2 in cancer. Clin Cancer Res, 2011. 17(9): p. 2613-8.

97. Caretti, G., et al., The Polycomb Ezh2 methyltransferase regulates muscle gene expression and skeletal muscle differentiation. Genes Dev, 2004. 18(21): p. 2627-38.

98. Wilkinson, F.H., K. Park, and M.L. Atchison, Polycomb recruitment to DNA in vivo by the YY1 REPO domain. Proc Natl Acad Sci U S A, 2006. 103(51): p. 19296-301.

99. Van Dessel, N., et al., The phosphatase interactor NIPP1 regulates the occupancy of the histone methyltransferase EZH2 at Polycomb targets. Nucleic Acids Res, 2010. 38(21): p. 7500-12.

100. Simon, J.A. and C.A. Lange, Roles of the EZH2 histone methyltransferase in cancer epigenetics. Mutat Res, 2008. 647(1-2): p. 21-9.

101. Yang, Y.A. and J. Yu, EZH2, an epigenetic driver of prostate cancer. Protein Cell, 2013. 4(5): p. 331-41.

102. Hussain, M., et al., Tobacco smoke induces polycomb-mediated repression of Dickkopf-1 in lung cancer cells. Cancer Res, 2009. 69(8): p. 3570-8.

103. Varambally, S., et al., Genomic loss of microRNA-101 leads to overexpression of histone methyltransferase EZH2 in cancer. Science, 2008. 322(5908): p. 1695-9.

104. Cao, P., et al., MicroRNA-101 negatively regulates Ezh2 and its expression is modulated by androgen receptor and HIF-1alpha/HIF-1beta. Mol Cancer, 2010. 9: p. 108.

105. Vancheri, C., Common pathways in idiopathic pulmonary fibrosis and cancer. Eur Respir Rev, 2013. 22(129): p. 265-72.

106. Vancheri, C., et al., Idiopathic pulmonary fibrosis: a disease with similarities and links to cancer biology. Eur Respir J, 2010. 35(3): p. 496-504.

107. Kasai, H., et al., TGF-beta1 induces human alveolar epithelial to mesenchymal cell transition (EMT). Respir Res, 2005. 6: p. 56.

108. Wakefield, L.M., et al., Transforming growth factor-beta1 circulates in normal human plasma and is unchanged in advanced metastatic breast cancer. Clin Cancer Res, 1995. 1(1): p. 129-36.

109. Shi, R. and V.L. Chiang, Facile means for quantifying microRNA expression by real-time PCR. Biotechniques, 2005. 39(4): p. 519-25.

110. Weng, T., et al., Regulation of lung surfactant secretion by microRNA-150. Biochem Biophys Res Commun, 2012. 422(4): p. 586-9.

111. Wang, Y., et al., Identification of rat lung-specific microRNAs by micoRNA microarray: valuable discoveries for the facilitation of lung research. BMC Genomics, 2007. 8: p. 29.

112. Chen, Z. and L. Liu, RealSpot: software validating results from DNA microarray data analysis with spot images. Physiol Genomics, 2005. 21(2): p. 284-91.

113. Bruce, M.C., C.E. Honaker, and R.J. Cross, Lung fibroblasts undergo apoptosis following alveolarization. Am J Respir Cell Mol Biol, 1999. 20(2): p. 228-36.

114. Homolya, L., et al., Nucleotide-regulated calcium signaling in lung fibroblasts and epithelial cells from normal and P2Y(2) receptor (-/-) mice. J Biol Chem, 1999. 274(37): p. 26454-60.

115. Ashcroft, T., J.M. Simpson, and V. Timbrell, Simple method of estimating severity of pulmonary fibrosis on a numerical scale. J Clin Pathol, 1988. 41(4): p. 467-70.

116. Chen, Z., et al., Identification of rat lung--prominent genes by a parallel DNA microarray hybridization. BMC Genomics, 2006. 7: p. 47.

117. Chiang, P.K. and G.L. Cantoni, Perturbation of biochemical transmethylations by 3-deazaadenosine in vivo. Biochem Pharmacol, 1979. 28(12): p. 1897-902.

118. Glazer, R.I., et al., 3-Deazaneplanocin: a new and potent inhibitor of S-adenosylhomocysteine hydrolase and its effects on human promyelocytic leukemia cell line HL-60. Biochem Biophys Res Commun, 1986. 135(2): p. 688-94.

119. Glazer, R.I., et al., 3-Deazaneplanocin A: a new inhibitor of S-adenosylhomocysteine synthesis and its effects in human colon carcinoma cells. Biochem Pharmacol, 1986. 35(24): p. 4523-7.

120. Liu, S., M.S. Wolfe, and R.T. Borchardt, Rational approaches to the design of antiviral agents based on S-adenosyl-L-homocysteine hydrolase as a molecular target. Antiviral Res, 1992. 19(3): p. 247-65.

121. Chiang, P.K., Biological effects of inhibitors of S-adenosylhomocysteine hydrolase. Pharmacol Ther, 1998. 77(2): p. 115-34.

122. Bell, E., B. Ivarsson, and C. Merrill, Production of a tissue-like structure by contraction of collagen lattices by human fibroblasts of different proliferative potential in vitro. Proc Natl Acad Sci U S A, 1979. 76(3): p. 1274-8.

123. Montesano, R. and L. Orci, Transforming growth factor beta stimulates collagen-matrix contraction by fibroblasts: implications for wound healing. Proc Natl Acad Sci U S A, 1988. 85(13): p. 4894-7.

124. Yang, S., et al., miR-31 is a negative regulator of fibrogenesis and pulmonary fibrosis. FASEB J, 2012. 26(9): p. 3790-9.

125. Duffy, H.S., Fibroblasts, myofibroblasts, and fibrosis: fact, fiction, and the future. J Cardiovasc Pharmacol, 2011. 57(4): p. 373-5.

126. Kis, K., X. Liu, and J.S. Hagood, Myofibroblast differentiation and survival in fibrotic disease. Expert Rev Mol Med, 2011. 13: p. e27.

127. Hardie, W.D., S.W. Glasser, and J.S. Hagood, Emerging concepts in the pathogenesis of lung fibrosis. Am J Pathol, 2009. 175(1): p. 3-16.

128. Araya, J. and S.L. Nishimura, Fibrogenic reactions in lung disease. Annu Rev Pathol, 2010. 5: p. 77-98.

129. Hinz, B., et al., Alpha-smooth muscle actin expression upregulates fibroblast contractile activity. Mol Biol Cell, 2001. 12(9): p. 2730-41.

130. Hinz, B., Formation and function of the myofibroblast during tissue repair. J Invest Dermatol, 2007. 127(3): p. 526-37.

131. Tomasek, J.J., et al., Myofibroblasts and mechano-regulation of connective tissue remodelling. Nat Rev Mol Cell Biol, 2002. 3(5): p. 349-63.

132. Darby, I.A. and T.D. Hewitson, Fibroblast differentiation in wound healing and fibrosis. Int Rev Cytol, 2007. 257: p. 143-79.

133. Hu, B., Z. Wu, and S.H. Phan, Smad3 mediates transforming growth factor-beta-induced alpha-smooth muscle actin expression. Am J Respir Cell Mol Biol, 2003. 29(3 Pt 1): p. 397-404.

134. Ramirez, A.M., et al., Myofibroblast transdifferentiation in obliterative bronchiolitis: tgf-beta signaling through smad3-dependent and -independent pathways. Am J Transplant, 2006. 6(9): p. 2080-8.

135. Cogan, J.G., et al., Vascular smooth muscle alpha-actin gene transcription during myofibroblast differentiation requires Sp1/3 protein binding proximal to the MCAT enhancer. J Biol Chem, 2002. 277(39): p. 36433-42.

136. Noseda, M., et al., Smooth Muscle alpha-actin is a direct target of Notch/CSL. Circ Res, 2006. 98(12): p. 1468-70.

137. Hu, B., et al., An essential role for CCAAT/enhancer binding protein beta in bleomycin-induced pulmonary fibrosis. J Pathol, 2007. 211(4): p. 455-62.

138. Hu, B., et al., Gut-enriched Kruppel-like factor interaction with Smad3 inhibits myofibroblast differentiation. Am J Respir Cell Mol Biol, 2007. 36(1): p. 78-84.

139. Feng, X.H. and R. Derynck, Specificity and versatility in tgf-beta signaling through Smads. Annu Rev Cell Dev Biol, 2005. 21: p. 659-93.

140. Nakao, A., et al., Identification of Smad7, a TGFbeta-inducible antagonist of TGF-beta signalling. Nature, 1997. 389(6651): p. 631-5.

141. Miyazono, K., Positive and negative regulation of TGF-beta signaling. J Cell Sci, 2000. 113 (Pt 7): p. 1101-9.

142. Tang, L.Y., et al., Ablation of Smurf2 reveals an inhibition in TGF-beta signalling through multiple mono-ubiquitination of Smad3. EMBO J, 2011. 30(23): p. 4777-89.

143. Lin, X., M. Liang, and X.H. Feng, Smurf2 is a ubiquitin E3 ligase mediating proteasome-dependent degradation of Smad2 in transforming growth factor-beta signaling. J Biol Chem, 2000. 275(47): p. 36818-22.

144. Zhang, Y., et al., Regulation of Smad degradation and activity by Smurf2, an E3 ubiquitin ligase. Proc Natl Acad Sci U S A, 2001. 98(3): p. 974-9.

145. Massague, J., J. Seoane, and D. Wotton, Smad transcription factors. Genes Dev, 2005. 19(23): p. 2783-810.

146. Kavsak, P., et al., Smad7 binds to Smurf2 to form an E3 ubiquitin ligase that targets the TGF beta receptor for degradation. Mol Cell, 2000. 6(6): p. 1365-75.

147. Nawshad, A., et al., Transforming growth factor-beta signaling during epithelial-mesenchymal transformation: implications for embryogenesis and tumor metastasis. Cells Tissues Organs, 2005. 179(1-2): p. 11-23.

148. Fujiwara, T., et al., 3-Deazaneplanocin A (DZNep), an inhibitor of S-adenosylmethionine-dependent methyltransferase, promotes erythroid differentiation. J Biol Chem, 2014. 289(12): p. 8121-34.

149. Kikuchi, J., et al., Epigenetic therapy with 3-deazaneplanocin A, an inhibitor of the histone methyltransferase EZH2, inhibits growth of non-small cell lung cancer cells. Lung Cancer, 2012. 78(2): p. 138-43.

150. Fiskus, W., et al., Combined epigenetic therapy with the histone methyltransferase EZH2 inhibitor 3-deazaneplanocin A and the histone deacetylase inhibitor panobinostat against human AML cells. Blood, 2009. 114(13): p. 2733-43.

151. Antoniou, K.M., et al., Idiopathic pulmonary fibrosis and lung cancer: a clinical and pathogenesis update. Curr Opin Pulm Med, 2015. 21(6): p. 626-33.

152. Mazieres, J., et al., Wnt signaling in lung cancer. Cancer Lett, 2005. 222(1): p. 1-10.

153. Chilosi, M., et al., Aberrant Wnt/beta-catenin pathway activation in idiopathic pulmonary fibrosis. Am J Pathol, 2003. 162(5): p. 1495-502.

154. Lovat, F., N. Valeri, and C.M. Croce, MicroRNAs in the pathogenesis of cancer. Semin Oncol, 2011. 38(6): p. 724-33.

155. Oak, S.R., et al., A micro RNA processing defect in rapidly progressing idiopathic pulmonary fibrosis. PLoS One, 2011. 6(6): p. e21253.

156. Tan, J., et al., Pharmacologic disruption of Polycomb-repressive complex 2-mediated gene repression selectively induces apoptosis in cancer cells. Genes Dev, 2007. 21(9): p. 1050-63.

157. Cheng, L.L., et al., TP53 genomic status regulates sensitivity of gastric cancer cells to the histone methylation inhibitor 3-deazaneplanocin A (DZNep). Clin Cancer Res, 2012. 18(15): p. 4201-12.

158. Xie, Z., et al., Determinants of sensitivity to DZNep induced apoptosis in multiple myeloma cells. PLoS One, 2011. 6(6): p. e21583.

159. Fiskus, W., et al., Superior efficacy of a combined epigenetic therapy against human mantle cell lymphoma cells. Clin Cancer Res, 2012. 18(22): p. 6227-38.

160. Grotendorst, G.R., H. Okochi, and N. Hayashi, A novel transforming growth factor beta response element controls the expression of the connective tissue growth factor gene. Cell Growth Differ, 1996. 7(4): p. 469-80.

161. Adam, P.J., et al., Positive- and negative-acting Kruppel-like transcription factors bind a transforming growth factor beta control element required for expression of the smooth muscle cell differentiation marker SM22alpha in vivo. J Biol Chem, 2000. 275(48): p. 37798-806.

162. Schnabl, B., et al., The role of Smad3 in mediating mouse hepatic stellate cell activation. Hepatology, 2001. 34(1): p. 89-100.

163. Xu, L., et al., Msk is required for nuclear import of TGF-{beta}/BMP-activated Smads. J Cell Biol, 2007. 178(6): p. 981-94.

164. Yao, X., et al., Preferential utilization of Imp7/8 in nuclear import of Smads. J Biol Chem, 2008. 283(33): p. 22867-74.

165. Chen, X. and L. Xu, Specific nucleoporin requirement for Smad nuclear translocation. Mol Cell Biol, 2010. 30(16): p. 4022-34.

166. Kurisaki, A., et al., The mechanism of nuclear export of Smad3 involves exportin 4 and Ran. Mol Cell Biol, 2006. 26(4): p. 1318-32.

167. Dai, F., et al., Nuclear export of Smad2 and Smad3 by RanBP3 facilitates termination of TGF-beta signaling. Dev Cell, 2009. 16(3): p. 345-57.

168. Hill, C.S., Nucleocytoplasmic shuttling of Smad proteins. Cell Res, 2009. 19(1): p. 36-46.

169. Dupont, S., et al., FAM/USP9x, a deubiquitinating enzyme essential for TGFbeta signaling, controls Smad4 monoubiquitination. Cell, 2009. 136(1): p. 123-35.

170. Kretzschmar, M., J. Doody, and J. Massague, Opposing BMP and EGF signalling pathways converge on the TGF-beta family mediator Smad1. Nature, 1997. 389(6651): p. 618-22.

171. Sapkota, G., et al., Balancing BMP signaling through integrated inputs into the Smad1 linker. Mol Cell, 2007. 25(3): p. 441-54.

172. Schmierer, B. and C.S. Hill, Kinetic analysis of Smad nucleocytoplasmic shuttling reveals a mechanism for transforming growth factor beta-dependent nuclear accumulation of Smads. Mol Cell Biol, 2005. 25(22): p. 9845-58.

173. Varelas, X., et al., TAZ controls Smad nucleocytoplasmic shuttling and regulates human embryonic stem-cell self-renewal. Nat Cell Biol, 2008. 10(7): p. 837-48.

174. Varelas, X., et al., The Crumbs complex couples cell density sensing to Hippo-dependent control of the TGF-beta-SMAD pathway. Dev Cell, 2010. 19(6): p. 831-44.

175. Wang, A., et al., Cutting edge: Smad2 and Smad4 regulate TGF-beta-mediated Il9 gene expression via EZH2 displacement. J Immunol, 2013. 191(10): p. 4908-12.

176. Degryse, A.L. and W.E. Lawson, Progress toward improving animal models for idiopathic pulmonary fibrosis. Am J Med Sci, 2011. 341(6): p. 444-9.

177. Moeller, A., et al., The bleomycin animal model: a useful tool to investigate treatment options for idiopathic pulmonary fibrosis? Int J Biochem Cell Biol, 2008. 40(3): p. 362-82.

178. DuPage, M., A.L. Dooley, and T. Jacks, Conditional mouse lung cancer models using adenoviral or lentiviral delivery of Cre recombinase. Nat Protoc, 2009. 4(7): p. 1064-72.

179. Coulombe, R.A., Jr., R.P. Sharma, and J.W. Huggins, Pharmacokinetics of the antiviral agent 3-deazaneplanocin A. Eur J Drug Metab Pharmacokinet, 1995. 20(3): p. 197-202.

180. Smits, M., et al., Down-regulation of miR-101 in endothelial cells promotes blood vessel formation through reduced repression of EZH2. PLoS One, 2011. 6(1): p. e16282.

181. Zhou, J., et al., The histone methyltransferase inhibitor, DZNep, up-regulates TXNIP, increases ROS production, and targets leukemia cells in AML. Blood, 2011. 118(10): p. 2830-9.

182. Crea, F., et al., Pharmacologic disruption of Polycomb Repressive Complex 2 inhibits tumorigenicity and tumor progression in prostate cancer. Mol Cancer, 2011. 10: p. 40.

183. Tan, J., et al., EZH2: biology, disease, and structure-based drug discovery. Acta Pharmacol Sin, 2013. 35: p. 161–174.

VITA

XIAO Xiao

Candidate for the Degree of

Doctor of Philosophy

Thesis: EPITHELIAL-TO-MESENCHYMAL TRANSITION AND FIBROBLAST DIFFERENTIATION IN IDIOPATHIC PULMONARY FIBROSIS

Major Field: Veterinary Biomedical Sciences (Physiology)

Biographical:

Education:

Completed the requirements for the Doctor of Philosophy in Veterinary Biomedical Sciences (Physiology) at Oklahoma State University, Stillwater, Oklahoma in December, 2015.

Master of Medicine in Clinical Medicine, Sun Yat-Sen University, Guangzhou, Guangdong, China 2009

Bachelor of Medicine in Ophthalmology, Sun Yat-Sen University, Guangzhou, Guangdong, China 2007

Experience:

Graduate Research Associate, Oklahoma State University, 2009-2015

Graduate Resident, Zhongshan Ophthalmic Center, Sun Yat-Sen University, Guangzhou, Guangdong, China, 2007-2009

Intern, First Affiliated Hospital of Sun Yat-Sen University, Sun Yat-Sen University, Guangzhou, Guangdong, China, 2006-2007

Professional Memberships:

American Thoracic Society (2011-2013)

American Association for the Advancement of Science (2009-2013)